

Citation

J. Quesada, C. Zhou, P. Chowdhury, M. Alotaibi, A. Mustafa, Y. Kumamnov, M. Prabhushankar, and G. AlRegib, "A Large-scale Benchmark on Geological Fault Delineation Models: Domain Shift, Training Dynamics, Generalizability, Evaluation and Inferential Behavior", submitted to IEEE Access

Review

Date of submission: 12 may 2025

Bib

@ARTICLE{Quesada2025Largescale,
author={J. Quesada and C. Zhou and P.Chowdhury and M. Alotaibi and A. Mustafa and Y. Kumamnov and M. Prabhushankar and G. AlRegib},
journal={IEEE Access},
title={A Large-scale Benchmark on Geological Fault Delineation Models: Domain Shift, Training Dynamics, Generalizability, Evaluation and Inferential Behavior},
year={2025},}

Copyright

©Creative Commons Attribution CCBY 4.0

Contact

olives.gatech@gmail.com

<https://alregib.ece.gatech.edu/>

A Large-scale Benchmark on Geological Fault Delineation Models: Domain Shift, Training Dynamics, Generalizability, Evaluation and Inferential Behavior

JORGE QUESADA¹, CHEN ZHOU¹, PRITHWIJIT CHOWDHURY¹, MOHAMMAD ALOTAIBI¹, AHMAD MUSTAFA², YUSUFJON KUMAKOV³, MOHIT PRABHUSHANKAR (MEMBER, IEEE)¹, and GHASSAN ALREGIB (FELLOW, IEEE)¹,

¹OLIVES at the Georgia Institute of Technology

²Occidental Petroleum Corporation

³Tashkent State Technical University

Corresponding author: Jorge Quesada (e-mail: jpacora3@gatech.edu).

This work is supported by the ML4Seismic Industry Partners at Georgia Tech

ABSTRACT Machine learning has taken a critical role in seismic interpretation workflows, especially in fault delineation tasks. However, despite the recent proliferation of pretrained models and synthetic datasets, the field still lacks a systematic understanding of the generalizability limits of these models across seismic data representing a variety of geologic, acquisition and processing settings. Distributional shifts between different data sources, limitations in fine-tuning strategies and labeled data accessibility, and inconsistent evaluation protocols all represent major roadblocks in the deployment of reliable and robust models in real-world exploration settings. In this paper, we present the first large-scale benchmarking study explicitly designed to provide answers and guidelines for domain shift strategies in seismic interpretation. Our benchmark encompasses over 200 models trained and evaluated on three heterogeneous datasets (synthetic and real data) including FaultSeg3D, CRACKS, and Thebe. We systematically assess pretraining, fine-tuning, and joint training strategies under varying degrees of domain shift. Our analysis highlights the fragility of current fine-tuning practices, the emergence of catastrophic forgetting, and the challenges of interpreting performance in a systematic manner. We establish a robust experimental baseline to provide insights into the tradeoffs inherent to current fault delineation workflows, and shed light on directions for developing more generalizable, interpretable and effective machine learning models for seismic interpretation. The insights and analyses reported provide a set of guidelines on the deployment of fault delineation models within seismic interpretation workflows.

INDEX TERMS Benchmarking, Domain shift, Seismic fault delineation, Seismic interpretation

I. INTRODUCTION

RECENT advances in machine learning (ML) have brought about a tectonic shift in the seismic interpretation workflow. ML-assisted approaches are leveraged in different parts of the pipeline, specifically in automated fault detection. Faults are geologically critical features that control fluid flow in Earth's subsurface, influence reservoir compartmentalization, and pose drilling hazards in hydrocarbon exploration [1], [2]. Beyond the energy sector, faults play a central role in earthquake nucleation and propagation, as well as geohazard and risk assessment in tectonically active regions

[3], [4]. Accurate and scalable fault interpretation is therefore a high-impact task across several geoscience domains. Early ML work in this area often repurposed semantic segmentation models from computer vision (such as those developed for natural images) to detect discontinuities in seismic sections. However, these generic frameworks struggled with the unique characteristics of seismic data, particularly the thin, curvilinear geometry of faults and the presence of acquisition artifacts and structural noise. As a result, the field has increasingly shifted toward fault delineation, a task-specific variant of segmentation that emphasizes the extraction of coherent

fault structures rather than general pixel-wise classification. This shift has prompted the development of domain-specific feature encoders, adapted loss functions, and structural priors that better capture the morphological signatures of faults [5], [6]. In general, the growing availability of ML methods has accelerated the adoption of data-driven interpretations that have provided new insights into fault structures within large seismic volumes [5], [6].

An ML-assisted seismic interpretation pipeline is illustrated in Fig. 1. In a standard workflow, interpreters at a new site begin by leveraging existing labeled datasets or synthetically generated volumes to train machine learning models. These models capture broad geophysical patterns and serve as a foundational prior, which can then be adapted to the new site through fine-tuning on a smaller set of locally interpreted seismic data. After fine-tuning, the models are evaluated within a consistent framework to ensure that their outputs align with geological expectations and interpretation standards. The validated predictions subsequently guide subsurface decision-making, and the new volume may in turn contribute to the pool of training data for future sites. However, while conceptually straightforward, this workflow embeds multiple assumptions and design choices that present significant challenges in practice, which we highlight in light blue in the diagram.

We further illustrate these challenges in Fig. 2: two central and intertwined challenges in the interpretation pipeline arise from the diversity of data sources (Fig. 2 (a)) and the strategies used to adapt models across them (Fig. 2 (b)). Seismic datasets differ widely in their geological characteristics, acquisition parameters, and resolution, among other factors. Synthetic data, while providing a fully specified ground truth, often fails to capture the complexity and variability of field data. Prior datasets from other regions, though more realistic, may still differ significantly from new target volumes. These domain shifts, whether from synthetic-to-real or across real-world basins, can cause pretrained models to generalize poorly to new sites [7], and eventually provide weak performance for the interpretation task.

To address the challenge of domain adaptation, researchers have proposed a variety of methods that address the effects of domain differences along the pipeline. Several studies introduce enhancements to model architectures [8], dataset construction [1], [9]–[11], uncertainty estimation [12] or explore training strategies aimed at improving data efficiency and transferability [13], [14]. A common approach involves pretraining models on synthetic data and subsequently fine-tuning them on real seismic volumes, as in [1]. More recent methods have explored using self-supervised learning to learn robust features without large amounts of labeled data [15]–[20], or adapting large vision foundation models trained on natural images to the seismic domain [6], [21], [22]. While these approaches offer promising results, their effectiveness is often dependent on the compatibility between source and target domains, and they remain vulnerable to issues such as catastrophic forgetting [23] during adaptation. Moreover, the

success of these approaches is influenced by several factors such as architecture and training design choices, as well as dataset-specific properties such as seismic section resolution, heterogeneity, and sample size.

Fig. 2(b) showcases a simple example of these aforementioned issues. The figure contains two rows, each displaying three seismic sections. The first row presents the output of three segmentation models commonly used in the seismic community, trained under the same settings with the same training data. We can observe that the three predictions differ significantly from each other. In the second row of Fig. 2(b), three segmentation outputs are shown after applying three different fine-tuning strategies. The first output in the second row is obtained by a model trained from scratch on the target data, while the other two are produced by models pretrained on other (larger) datasets and then finetuned on the target data. We further conduct objective evaluation of these outputs and summarize these metrics in Fig. 3. The y-axis in this figure is the average Hausdorff distance between the output of the model and the ground truth, where smaller values signify better predictions. There are four strategies shown. The first one is where the model is trained on the target volume. The second strategy is to use a model that was trained on a real dataset and fine-tune it on the target dataset. The third strategy is to use a model that was trained in a synthetic dataset and then fine-tuned on the target dataset. These three strategies match the three depicted in Fig. 2(b). A fourth strategy is to use a model that was jointly trained on both synthetic and real data, then fine-tuned on the target data. Although we will discuss these experiments in more detail later in the paper, the figure here shows the large difference in performance across these four strategies. For now, this shows that despite this growing body of work, the field still lacks a systematic understanding of when, how, and why a given strategy outperforms others under domain shift. This paper is the first attempt, to our knowledge, within the community to provide answers and guidelines for domain shift strategies in seismic interpretation.

The third critical complication in the pipeline arises in evaluation, as depicted in Fig. 2(c). Fault labels are derived from expert interpretation and are often subjective [24], [25], particularly in complex or ambiguous structural settings. This subjectivity leads to inconsistencies in ground truth across datasets or among annotators, and complicates objective model evaluation. Furthermore, a given metric may penalize correct but unannotated predictions, while failing to reflect geological plausibility or structural consistency [5], [26]. To address this, our study provides an in-depth analysis of commonly used evaluation metrics (such as Dice coefficient, Chamfer and Hausdorff distances) in the context of fault interpretation. This analysis highlights the need for a more holistic evaluation approach that integrates quantitative measures with geological interpretability.

This paper presents a large-scale benchmarking study regarding the performance variability of over 200 fault delineation models across training regimes, data characteristics,

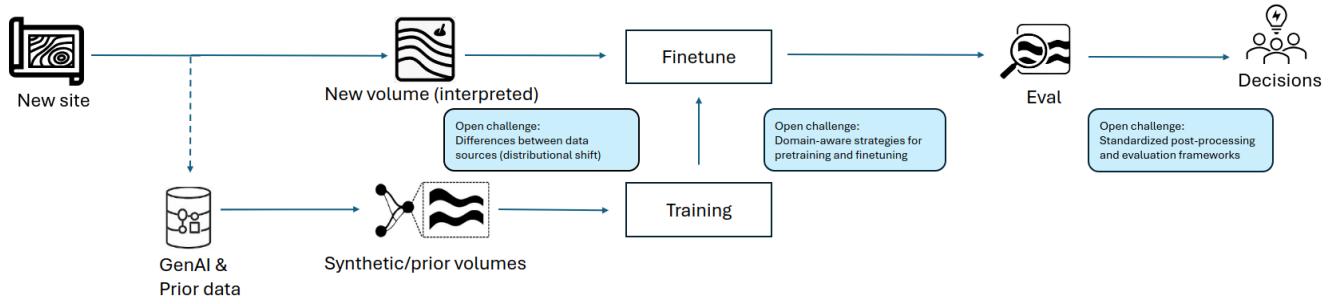
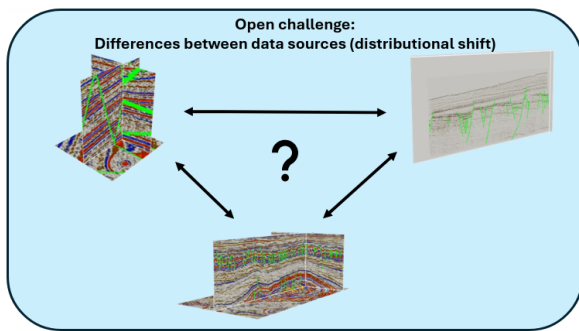
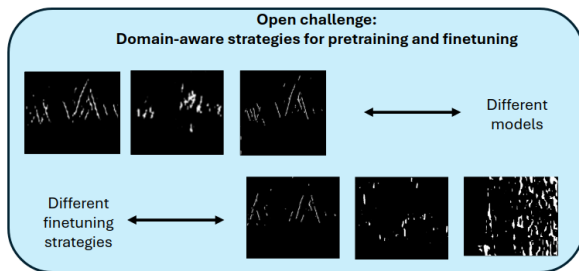


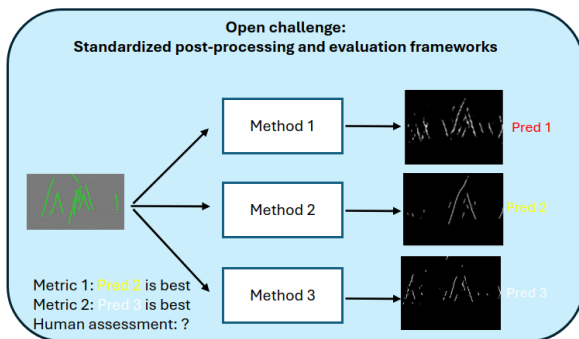
FIGURE 1: Typical ML-assisted seismic interpretation workflow



(a) Distributional Shift



(b) Domain-aware Fine-tuning



(c) Standardized Evaluation

FIGURE 2: Existing challenges in the current interpretation workflow

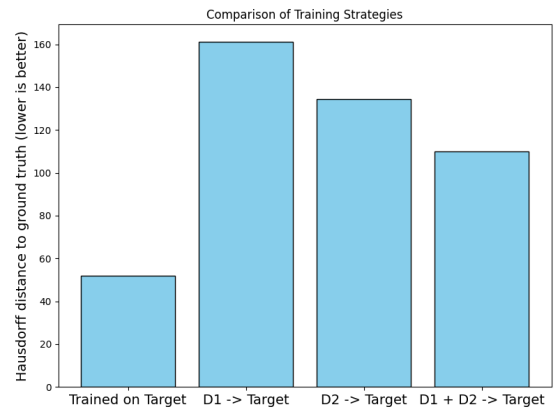


FIGURE 3: Finetuning example from a real dataset (D1) and a synthetic dataset (D2) to a target real dataset

and architectural choices. These fault delineation models include a combination of eight deep learning architectures, trained and fine-tuned on three distinct datasets, including both synthetic and real volumes. Our experiments cover a broad spectrum of training strategies, including pretraining on a single fault dataset, pre-training on large-scale natural image dataset such as ImageNet [27], using randomly initialized models, and jointly training on multiple fault datasets. We shed light on the impact of these training strategies, with a focus on three critical challenges in the seismic machine learning domain: model generalizability under domain shift, training dynamics, and evaluation robustness. The results of our extensive study allow the community to examine the limitations of the current seismic interpretation pipelines, and underscore the need for a framework that integrates both quantitative metrics and qualitative expert review. We identify failure cases and inconsistencies in fault delineation tasks, and thus highlight the need for interpretability and domain-awareness in model design and evaluation. We provide a succinct highlight of the key observations of our benchmarking experiments in Table 2.

II. RELATED WORK

The structure of this section mirrors the stages outlined in Fig. 1. Existing literature on machine learning for fault

delineation follows a similar modular approach: beginning with data preprocessing and input normalization, proceeding through model training, adaptation strategies and inferential behavior, and culminating in evaluation protocols. In this section, we review prior work organized along these stages, highlighting how each component contributes to generalization across seismic domains.

A. DATA PREPARATION AND PREPROCESSING

In computer vision segmentation pipelines, raw images from natural scenes [28]–[30] and medical scans [31]–[33] are first standardized to ensure consistent spatial dimensions and intensity distributions [34], [35]. Typical preprocessing steps include resizing or cropping to a fixed height and width, data augmentation, whitening [36], and contrast adjustments to mitigate variability in lighting or sensor settings [37], [38]. These operations guarantee that each input conforms to the network’s architectural requirements and that learned features are not biased by extraneous intensity fluctuations.

Seismic segmentation extends these practices to volumetric data acquired in formats such as SEG-Y (.sgy), raw binary (.dat), or serialized NumPy arrays (.npz). A common workflow begins by reading trace headers to assemble a 3D volume of dimensions (inline \times xline \times time/depth), and either processing the volume at that level [1], [5] or extracting 2D inline or crossline sections for further processing [9], [18]. To enlarge the training set and fit GPU memory constraints, each section is tiled with an overlapping sliding window of size $H \times W$ pixels (the effects of different tiling standards are studied and results presented in Section V-B1.).

Since raw seismic amplitudes can span orders of magnitude and contain acquisition artifacts, it is a standard practice to normalize each volume either via min–max scaling or z-score transformation. For min–max, each amplitude v_{ij} becomes

$$v'_{ij} = 2 \frac{v_{ij} - \lambda_{\min}}{\lambda_{\max} - \lambda_{\min}} - 1, \quad (1)$$

where λ_{\min} and λ_{\max} are the global minimum and maximum amplitudes in the volume. Alternatively, z-score normalization

$$v''_{ij} = \frac{v_{ij} - \mu}{\sigma} \quad (2)$$

centers the data to zero mean and unit variance, with μ and σ computed over all voxels. Fault masks (either interpreter-drawn or synthetically generated) are saved as binary images (.png or .npy) and cropped identically to their corresponding seismic windows. This systematic preprocessing pipeline (from raw SEG-Y/DAT ingestion, through standardized normalization and windowed slicing, to precisely aligned input–mask pairs) provides a consistent basis for benchmarking and comparing fault delineation models across diverse seismic domains.

B. TRAINING DYNAMICS AND SETUPS

Popular network choices designed for natural image segmentation are sensitive to training and design choices like model

architecture, input window size, and loss functions. Networks such as U-Net [31], DeepLab [29], and SegFormer [39] typically accept fixed-size patches (e.g., 256×256 or 512×512 pixels), balancing the need for sufficient context against GPU memory limits. During each training iteration, these patches are sampled, sometimes at multiple scales to expose the network to varied object sizes and to regularize against overfitting. Segmentation models optimize losses designed to reconcile pixel-wise accuracy with region-level coherence. For binary masks, a commonly used loss is the pixel-wise binary cross-entropy (BCE) [40], given as follows:

$$\mathcal{L}_{\text{BCE}} = -\frac{1}{N} \sum_{i=1}^N [y_i \log(p_i) + (1 - y_i) \log(1 - p_i)], \quad (3)$$

where p_i is the predicted probability at pixel i , $y_i \in \{0, 1\}$ is the ground-truth label, and N is the number of pixels in the patch. An alternative that tends to better adapt to settings with class imbalance and emphasize overlap is the Dice loss [41] given as follows:

$$\mathcal{L}_{\text{Dice}} = 1 - \frac{2 \sum_{i=1}^N p_i y_i + \epsilon}{\sum_{i=1}^N p_i + \sum_{i=1}^N y_i + \epsilon}, \quad (4)$$

where ϵ is a small constant to provide numerical stability. The BCE loss emphasizes the pixel fidelity while the Dice loss takes the overlap into consideration. Therefore, hybrid objectives combining BCE and Dice, e.g. $\mathcal{L} = \alpha \mathcal{L}_{\text{BCE}} + (1 - \alpha) \mathcal{L}_{\text{Dice}}$, are commonplace to leverage both pixel fidelity and region overlap [42], [43].

In seismic fault delineation, similar principles apply but with additional considerations. Input patches are typically larger to capture fault continuity across sections, and training often uses overlapping windows with a stride smaller than the patch size to ensure boundary faults are adequately sampled [1], [44]–[46]. The aforementioned loss functions, coupled with learning rate schedules and different regularization functions, form the backbone of seismic training setups [47]–[49]. By carefully tuning window sizes and loss compositions, researchers mitigate class imbalance and preserve structural continuity in fault delineation [50].

C. GENERALIZATION AND TRANSFERABILITY

Generalization refers to a model’s ability to maintain performance when presented with new, unseen data that (ideally) follows the same distribution as the training set [51]–[53]. In segmentation, this means accurately delineating objects or regions under variations in lighting, scale, or background texture. However, a common obstacle to generalization is domain shift, which occurs when the statistical properties of training and test data differ (such as changes in camera sensors or scene composition) often leading to degraded performance [54]–[58]. Domain adaptation encompasses strategies to reduce this gap, for instance by aligning feature distributions between source and target domains [59], [60]. Another common technique to adapt to target domains is fine-tuning: a network pretrained on a large, generic dataset

(the source) is adapted to a more specialized task (the target) by retraining some or all layers, thereby leveraging learned representations while adjusting to new data characteristics [61], [62].

In seismic segmentation, generalization to new domains is particularly difficult due to variability in acquisition parameters, stratigraphy, frequency content, and noise levels across surveys. This is true for fault delineation, where subtle and discontinuous features are easily obscured by processing artifacts or geologic heterogeneity [47], [63]. Models trained on one domain (such as synthetic datasets like `FaultSeg3D` [1]) often fail to transfer effectively to real data from different basins. To mitigate such domain shift, researchers have explored domain adaptation techniques including feature-space alignment [64], adversarial learning [65], and seismic-style transfer [66]. Fault-specific approaches also include synthetic fault injection [67] and contrastive learning tailored to structural continuity [20]. Transfer learning pipelines typically rely on pretrained encoders (either from natural images [68], [69] or large-scale seismic simulations with domain-specific decoders [1], [47]) followed by fine-tuning on limited labeled sections. These strategies must navigate a tradeoff between plasticity and stability: aggressive weight updates are prone to inducing catastrophic forgetting [23], while conservative tuning may fail to capture domain-specific features. As a result, generalization in seismic fault delineation requires careful calibration of both model architecture and adaptation strategy to handle the subtle, spatially sparse structures across diverse geological, acquisition, and imaging settings.

D. INFERENCE BEHAVIOR

In semantic segmentation, inference entails mapping learned feature representations to discrete pixel-level predictions [28]. The fidelity of this mapping depends on the architecture's ability to aggregate context and fuse features: models with narrow receptive fields may accurately localize edges but miss global structure [31], while those with extensive context capture coherent regions at the expense of sharp boundaries [29]. During inference, the bias-variance tradeoff emerges as a tension between boundary precision and region consistency, sometimes mitigated by post-processing, e.g., Conditional Random Fields [70] or edge-aware refinement modules [71].

In seismic fault delineation, these inferential tendencies are amplified by the thin, curvilinear nature of faults and the high noise intrinsic to seismic volumes [63]. U-Net's symmetric encoder-decoder and skip connections excel at preserving local detail, producing crisp fault traces when the signal-to-noise ratio is high [31], but its reliance on local convolutions and fixed strides can fragment continuous faults under heteroskedastic noise [47]. DeepLab's atrous convolutions and Atrous Spatial Pyramid Pooling (ASPP) module gather multi-scale context, yielding smoother, globally coherent fault masks [29]; yet the dilation patterns can inadvertently merge adjacent non-fault discontinuities, introducing false positives along stratigraphic horizons [29]. Seg-

Former's transformer-based encoder captures long-range dependencies and adapts to complex fault geometries, enhancing continuity across sections [39]—though its patch-based attention can produce coarser boundaries if patch size is not carefully chosen [39]. These model-specific inferential biases drive distinct behaviors in fault delineation and inform the choice of architectures and post-processing strategies for robust seismic interpretation.

E. PERFORMANCE EVALUATION

Segmentation evaluation seeks to quantify how closely a predicted mask P approximates the ground-truth mask G as subsets of the image domain. Evaluation metrics are categorized in the following two ways: (i) region based measures, which treat masks as sets and quantify volumetric overlap, and (ii) distance-based measures, which treat masks as shapes and quantify geometric deviations along their contours.

Region-based metrics include the Jaccard index (also known as intersection-over-union):

$$\text{Jaccard}(P, G) = \frac{|P \cap G|}{|P \cup G|}, \quad (5)$$

and the Dice coefficient:

$$\text{Dice}(P, G) = \frac{2|P \cap G|}{|P| + |G|}, \quad (6)$$

which captures the proportion of shared pixels but may understate errors on thin or tortuous structures.

Distance-based metrics such as Hausdorff offer tolerance against spatial shifts, but they are sensitive to noisy outliers [72]. To mitigate this issue, the modified Hausdorff was proposed by Dubuisson and Jain [73] that considers the average distance to the nearest neighbor, rather than the maximum distance as in the traditional formulation. In [74], the authors utilize the Bidirectional Chamfer Distance (BCD) metric, which measures the minimum distance from each pixel in both directions. Although region based metrics such as the Dice coefficient are useful for assessing shape quality, from a geophysicist's perspective, evaluation should measure the structural similarity between lines rather than discrete points. The modified Hausdorff distance D_h and the BCD D_c between two non-empty sets P and G are defined respectively as:

$$D_h(P, G) = \max \left(\frac{1}{N_p} \sum_{p \in P} \min_{g \in G} \|p - g\|, \frac{1}{N_g} \sum_{g \in G} \min_{p \in P} \|g - p\| \right) \quad (7)$$

$$D_c(P, G) = \frac{1}{N_p} \sum_{p \in P} \min_{g \in G} \|p - g\|^2 + \frac{1}{N_g} \sum_{g \in G} \min_{p \in P} \|g - p\|^2 \quad (8)$$

where:

- $\|\cdot\|$ denotes the Euclidean norm.

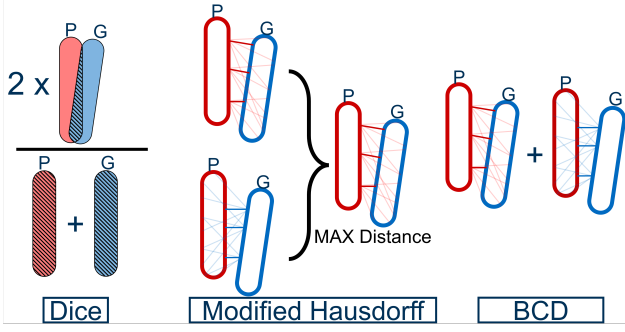


FIGURE 4: Differences between the considered metrics.

- $\min_{g \in G} \|p - g\|$ is the distance from point $p \in P$ to its nearest neighbor in G ,
- $\sum_{p \in P}$ and $\sum_{g \in G}$ are summations over all points in sets P and G , respectively,
- N_p and N_g are the number of elements in the sets P and G , respectively.

To illustrate the complementary nature of these metrics, we present a toy example in Fig. 4. The Dice coefficient measures spatial overlap by comparing each predicted pixel against the ground truth, yielding a single overlap score. In contrast, both the bidirectional Chamfer distance (BCD) and the modified Hausdorff distance assess boundary discrepancies: BCD sums the forward and reverse distances, whereas the modified Hausdorff takes the larger of the two. Because BCD and the modified Hausdorff yield nearly identical trends, our figures plot either one of them alongside the Dice coefficient.

III. FAULT DELINEATION DATASETS

Among all 74 datasets used for fault delineation [75], only 4 field datasets (LANDMASS [9], [76]–[82], GSB [45], [83], [84], Thebe [84], [85], CRACKS [86]) and 4 synthetic datasets (FaultSeg3D [1], Bi’s 3D synthetic [87], Wu’s 2D SR [88], Pochet’s 2D synthetic [89]) open-sourced both seismic data and labels. The low ratio of open-source labeled field data hinders the creation of benchmarks for training and evaluation of models.

Besides the lack of public availability, the different characteristics of the datasets pose challenges to the development of generalizable ML models. Specifically, LANDMASS contains image-level fault labels that cannot be used to numerically evaluate the delineation of pixel-wise faults. GSB contains pixel-wise fault labels annotated on only 5 crossline sections, which limits the evaluation scalability on large test data. Additionally, it is challenging to achieve generalization using only a small number of labels for finetuning [50]. In contrast, Thebe provides a large amount of pixel-level geophysicist labels across 1803 crossline sections. CRACKS provides fault labels of varying quality collected from a group of interpreters, including a geophysicist expert, across 400 inline sections.

Among the four publicly available datasets, we select Thebe and CRACKS considering the model development and evaluation at the pixel level. All the seismic sections in Pochet’s 2D synthetic contain only one straight fault crossing the entire section, presenting less diversity in angle and density compared to the faults in FaultSeg3D. Both Bi’s 3D synthetic and Wu’s 2D SR [88] originate from FaultSeg3D using the same synthesizing workflow. Thus, we use FaultSeg3D as a reference synthetic dataset with a diverse set of faults. Below we describe and compare the three datasets used for our benchmarking study in detail.

FaultSeg3D is a 3D synthetic dataset with 220 volumes each with dimensions of $128 \times 128 \times 128$ [1]. In order to better approximate realistic conditions, the authors added background noise estimated from real seismic volumes. The sampling rate and the frequency of the synthetic data vary across the volume to improve the diversity of the data. An example volume is shown in Fig. 5a.

CRACKS is an open-source dataset with diverse faults delineated across 400 inline sections of the Netherlands F3 Block [86], [90]. The authors in [10] open-sourced a fully-annotated 3D geological volume of the Netherlands F3 Block for training different models and comparing the performance with objective metrics. Thus, this volume is one of the most extensively studied geographical zones for developing ML-assisted seismic interpretation frameworks [2], [10], [12]–[14], [20], [22], [44]–[46], [48]–[50], [52], [53], [81], [82], [91]–[106]. The diverse fault features in the F3 block, including major versus minor faults and varying orientations, make it an excellent seismic dataset to train and evaluate fault delineation models [107], [108]. However, the annotations in [10] do not provide pixel-wise fault labels. Thus, CRACKS open-sources fully hand-labeled fault annotations by a group of 32 interpreters with varying degrees of expertise and a domain expert geophysicist. This dataset not only establishes a standardized benchmark for objective comparison but also can be used to investigate the impact of multiple sets of labels with varying quality. Three sets of fault annotations are used to investigate the impact of training labels with varying quality, including expert labels and two more sets of lower quality labels from two other annotators. Fig. 5b shows an example inline section with expert fault labels from CRACKS. CRACKS and FaultSeg3D share geological similarity in the seismic sections in addition to the similar label density.

Thebe is taken from a seismic survey called Thebe Gas Field in the Exmouth Plateau of the Carnarvan Basin on the NW shelf of Australia [11], [84]. The dataset contains 1803 labeled crossline sections of size 1737×3174 , making it the largest publicly-available field dataset. The seismic intensity of this dataset exhibits a low variation/standard deviation, which can be observed from the low contrast in Fig. 5c.

IV. EXPERIMENTAL SETUP

The workflow of ML-assisted fault delineation involves multiple choices including (i) the decision to fine-tune or not, (ii)

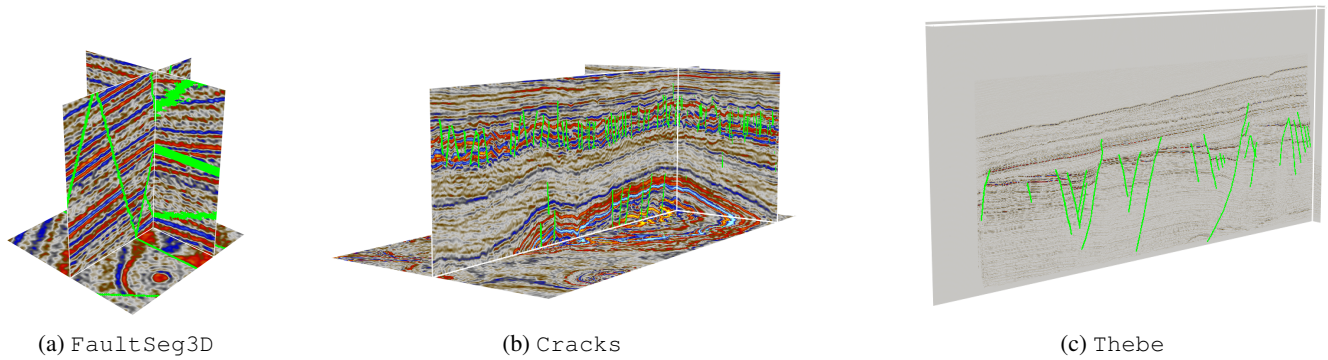


FIGURE 5: Visuals from three datasets: (a) synthesized faults in FaultSeg3D, (b) expert labels in CRACKS, and (c) expert labels in Thebe.

the selection of the datasets for pre-training and fine-tuning, (iii) the selection of different models, (iv) the development of pre-processing and post-processing strategies, and (v) the standardization of the evaluation protocols. We depict our systematic benchmarking pipeline in Fig. 6, which we use to holistically compare the impact of every choice and the various combinations of such choices. We provide details on each component of our pipeline in this section.

A. DATA PREPARATION

1) Standardizing Fault Annotations using Morphological Operations

There exist significant differences between the thickness of fault annotations in CRACKS, Thebe, and FaultSeg3D. We show three labeled patches of the same size from Thebe, CRACKS, and FaultSeg3D in Fig. 7a. The faults manually delineated by interpreters in Thebe and CRACKS are thicker than the synthesized faults in FaultSeg3D. The inconsistent thickness of fault annotations often influences model optimization, which typically uses pixel-based loss functions. However, existing workflows neglect this fault annotation inconsistency [84], [85], [88], [109]. The synthesized faults in FaultSeg3D precisely delineate the thin fractures in the seismic volumes. We therefore standardize the fault thickness across datasets by processing the manually delineated faults in Thebe and CRACKS to have the same thickness of the faults in FaultSeg3D. Specifically, we apply a simple sequence of morphological operations: we first skeletonize the raw fault annotations and then apply dilation with a rank-3 structural element to uniformize fault thickness and close any small gaps, as shown in Fig. 7b. This process is denoted by the Preprocess block in Fig. 6. We use standard Python libraries `scikit-image` and `scipy` for these morphological operations.

2) Training and Test Splits

To ensure meaningful evaluations, we adopt a consistent splitting strategy across the considered datasets. Specifically, we maximize diversity in the test set while ensuring no over-

lap with the training data. For each dataset, we select spatially distinct subsets to prevent redundancies and simulate deployment conditions on previously unseen segments. In CRACKS, which consists of 400 contiguous inlines, we designate the first 30 and last 30 sections as the test set, totaling 60 sections. The remaining 340 central sections are used for training. This split captures geological variability across the volume while maintaining spatial separation between training and test data. For Thebe, we use 400 sections for training and reserve 100 sections from other parts of the volume for testing, following a similar diversity-maximizing approach. For FaultSeg3D, we follow the established setup from [1], using 200 synthetic volumes for training and 20 distinct volumes for testing.

B. MODEL SETUP

We consider eight segmentation models commonly used in the seismic literature [5], [84], [88], [110] in our fault delineation experiments, using the following nomenclature:

- **deeplab**: Deeplab [111] architecture with a Resnet50 [68] backbone
- **deeplab-m**: Deeplab architecture with a Mobilenet [112] backbone
- **hed**: Holistically-nested edge detection model [113]
- **rcf**: Richer convolutional features [114]
- **unet**: Unet [31] architecture with a Resnet50 backbone
- **unet++**: Unet++ [115] architecture with a Resnet50 backbone
- **unet-b**: Original Unet architecture as presented in [31]
- **segformer**: Transformer-based model introduced in [39]

For each of these models, we perform all pairwise combinations of pretraining-finetuning settings between the 5 sets of labeled training data in the top left of Fig. 6. For example, a model is first pretrained on CRACKS-expert and then finetuned on all 5 datasets, resulting in 25 sets of weights for each considered model. Each of these model weights is then evaluated on CRACKS, Thebe, and FaultSeg3D.

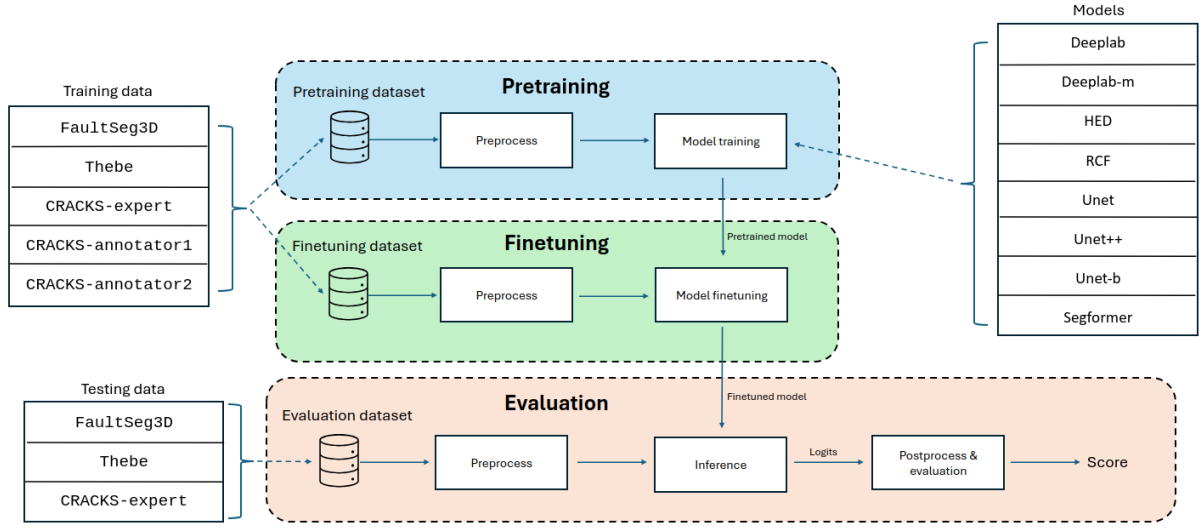
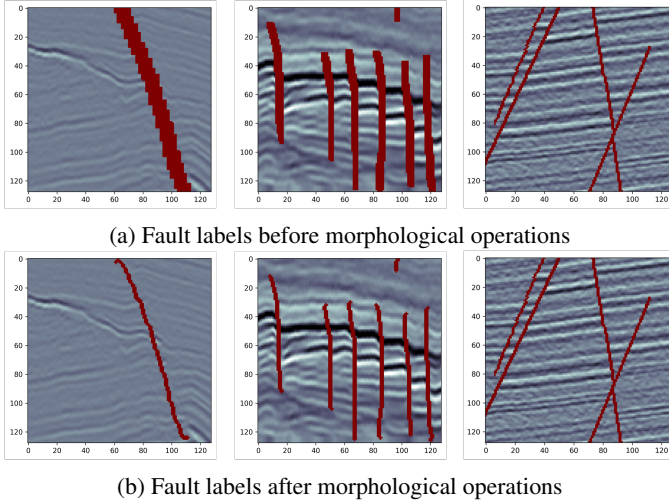


FIGURE 6: The block diagram of our experimental setup.

FIGURE 7: Example 128×128 patches of fault annotations with varying thickness in the three datasets. Left: Thebe, middle: CRACKS, right: FaultSeg3D

To complete our baselines, we also use four ImageNet-pretrained models and finetune them on our seismic datasets.

C. EVALUATION SETUP

1) Post-processing for Model Predictions

Common practices of evaluating deep fault delineation networks involve two steps [8], [50], [84], [85]: (i) thresholding the network predictions to obtain binary outputs, and (ii) comparing the binary outcomes with the fault test labels using a metric. The test labels are processed with the same morphological operations as the training faults in order to achieve consistent fault thickness at the input and output of a model. Consequently, the thresholding in step (i) needs to be

adaptive to the model and the data accordingly, followed by the same morphological operations for numerical evaluation. We compute the optimal threshold for the dataset using the Optimal Dataset Scale (ODS) metric [109]. For a model, its optimal threshold is computed using the training set, which is then applied to binarize the predictions on the test data, followed by the same morphological operation for evaluation.

2) Performance Metrics

As mentioned in Section II-E, pixel-based and distance-based metrics capture different aspects of prediction quality, and each can fail to fully reflect the structural accuracy of the predicted faults, making the evaluation of fault delineation methods an inherently challenging task. Our benchmark study thus adopts a holistic approach to assess prediction quality by considering a combination of multiple metrics alongside subjective inspection. In this study we choose to report one pixel-based metric, Dice Coefficient (defined in Eq. (6)) and two distance-based metrics: BCD and the modified Hausdorff (defined in Eq. 8, and Eq. 7, respectively), whose difference we showcased in Fig. 4. These metrics have not only been extensively used in the seismic literature for model performance assessment [1], [25], [73], but allow for two different evaluation axes: pixel overlap-based and structure-based.

V. RESULTS

Benchmarking results are analyzed across three different thematic axes: (1) generalizability and transferability, (2) training dynamics, and (3) metric evaluation.

A. GENERALIZATION AND TRANSFERABILITY

As mentioned in Section I, models are often used to process data from new surveys that can differ from their original training sources. As such, generalization and transferability

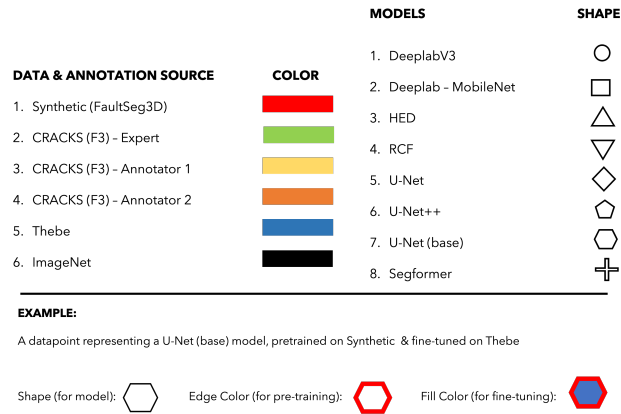


FIGURE 8: Visual encoding to represent the different models pretrained and finetuned on different datasets. Border color signifies the pretraining data source and the fill color signifies the fine-tuning dataset. Models are represented using various shapes.

are critical for reliable deployment and to reduce the labeling overhead. Understanding how various training regimes perform across domains is key to developing scalable workflows.

In this subsection, the generalization of models trained under different pretraining-finetuning regimes is analyzed across CRACKS, FaultSeg3D, and Thebe. Unless stated otherwise, we structure our scatter plots using the convention depicted in Fig. 8. The shape of a given point encodes the model used, the border color corresponds to the dataset used for pretraining the model, and the fill color corresponds to the datasets used for finetuning the model. All of our reported figures and plots correspond to models being evaluated in a held-out test partition of one of these 3 datasets.

1) Dataset Alignment and Transfer Trends

Figs. 9, 10 and 11 provide a macroscopic view of the model behaviors across the different training setups. On CRACKS (Fig. 9), the top-performing configurations are those pretrained on FaultSeg3D data and fine-tuned on CRACKS. The observation indicates strong geophysical commonalities between FaultSeg3D and CRACKS data, and supports the utility of FaultSeg3D data as a viable pretraining source when real annotations are limited. The fill-color distribution in Fig. 9 also establishes a hierarchy of effective finetuning datasets for CRACKS: CRACKS > FaultSeg3D > Thebe. The poor finetuning performance on Thebe indicates that it is more distributionally distant from CRACKS than FaultSeg3D data.

Furthermore, when tested on FaultSeg3D data (Fig. 10), models pretrained on CRACKS again outperform those trained from scratch, indicating that the aforementioned alignment is reciprocal. However, for Thebe (Fig. 11), top-performing models are those trained from scratch on Thebe itself. Transferring from either FaultSeg3D or CRACKS

results in performance degradation, suggesting that Thebe resides in a distinct feature space.

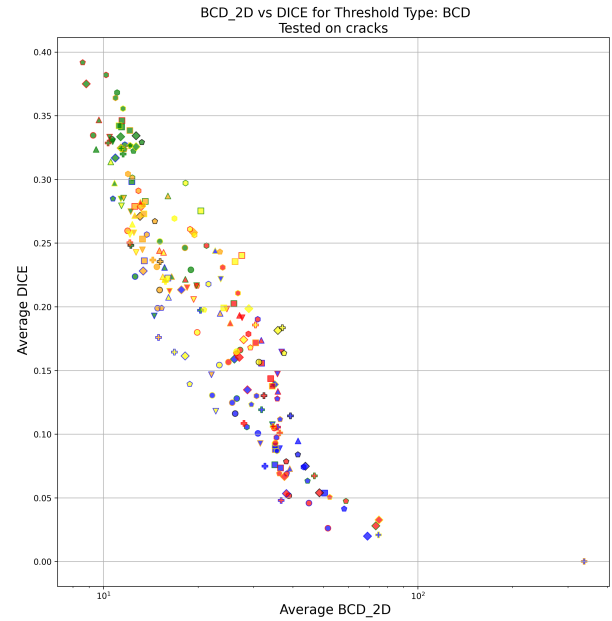


FIGURE 9: Test on CRACKS dataset

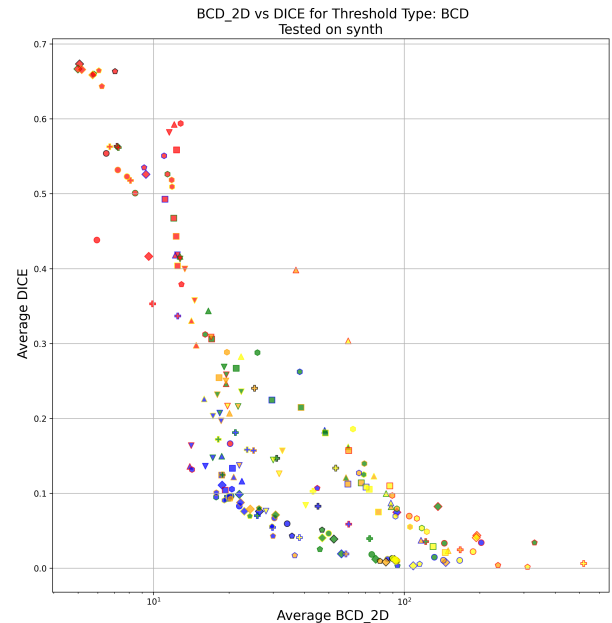


FIGURE 10: Test on FaultSeg3D dataset

2) Domain Shift and Joint Training

Domain shift is a pressing challenge in seismic ML, particularly when deploying models across surveys with different geological properties. When overlooked, this can lead to brittle models that perform well on training data but fail on new volumes, or models that catastrophically forget features from their original data after finetuning. An illustration of

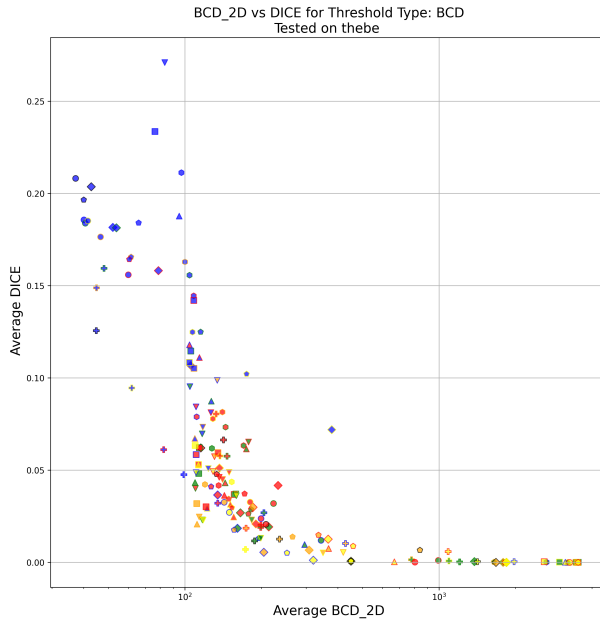


FIGURE 11: Test on Thebe dataset

this catastrophic forgetting occurs when models pretrained on CRACKS are fine-tuned on Thebe: despite reasonable performance on Thebe, these models experience dramatic performance degradation when re-evaluated on their original domain. In the case of *unet++*, for instance, the Dice score on CRACKS drops from 0.34 to 0.12, while the BCD increases twofold, indicating a complete erasure of useful representations, and clear case of catastrophic forgetting. A statistical analysis shows that Thebe has a significantly lower standard deviation (**0.124**) compared to CRACKS (**1.149**) and FaultSeg3D (**1.052**). The contrast and intensity variations in Thebe are lower, while CRACKS and FaultSeg3D have diverse intensity distributions, as shown in Fig. 5. An explanation for this catastrophic forgetting phenomenon is that models trained on Thebe learn from a constrained input range and struggle when tested on datasets with richer intensity distributions. These results suggest that other normalization techniques before training could help reduce these distributional mismatches.

As an additional baseline, experiments on joint training on all possible combinations of datasets in a single training round are conducted using the *unet* model with a ResNet50 backbone. The results for all *unet* experiments, including these joint training configurations, are shown in Table 1. The results further showcase that features learned from CRACKS and FaultSeg3D data align together, but these learned features are not easily transferable to Thebe. On the other hand, Thebe acts as a regularizer, hurting performance on seen datasets but providing modest generalization to unseen ones.

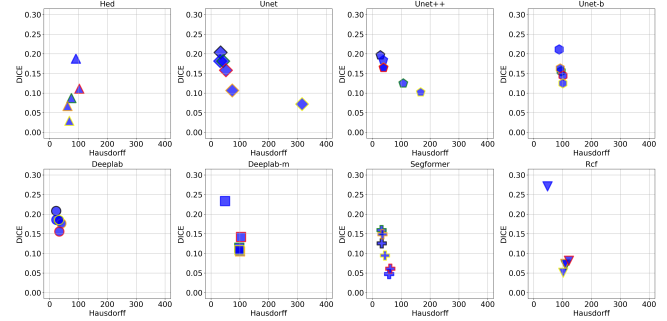


FIGURE 12: Individual Models tested on Thebe. Models with blue edges are pretrained on Thebe without finetuning. While other models are pretrained on different datasets. We show that pretraining on another faults dataset is not beneficial compared to using Imagenet weights or training from randomly initialized models.

3) Model Capacity and Transferability

It is generally established in the literature that pretraining on a large dataset can boost the performance of a model even in self-supervised settings [5]. However, in seismic applications, the benefits of pretraining are critically sensitive to the distributional similarity between the source and target domains—a phenomenon that reflects the strong coupling between geologic variability and model transferability. As shown in our experiments, models pretrained on FaultSeg3D or CRACKS and fine-tuned on Thebe underperform compared to models trained from scratch or initialized from ImageNet weights (Fig. 12). In such distributionally mismatched cases, the standard pretraining-finetuning strategy may hinder rather than help performance.

A factor that also plays a role in modulating generalization is model capacity. Fig. 12 and Fig. 13 show that large models like *segformer* benefit from pretraining on CRACKS, while smaller models (e.g., *hed*, *deeplab-m*) generalize better when trained from scratch. The observation suggests that both data alignment and model capacity affect transfer effectiveness.

Furthermore, models respond differently to fine-tuning. When pretraining on FaultSeg3D and fine-tuning on Thebe, models degrade in CRACKS performance. Fig. 14) shows that Thebe induces domain shifts that are hard to unlearn. Conversely, even though the finetuning dataset is distributionally closer to the target, Thebe-pretrained *segformer* and *deeplab* also degrade on CRACKS after finetuning on FaultSeg3D as shown in Fig. 14. The asymmetric behavior highlights the difficulty of finding universally robust pretraining strategies.

B. TRAINING DYNAMICS AND INFERENCE BEHAVIOR

In this section we analyze the impact of different training dynamics and model architectures on performance and inferential behavior.

TABLE 1: Performance Metrics (DICE, BCD, Hausdorff) for different training schemes on Unet. All values are rounded to three decimals. Schemes are ranked as best, second best or worst based on satisfying at least two of the three metric criteria, to account for cases where metrics disagree. (blue for highest, pink for second, and gray for the worst.)

Training Configuration	Test on FaultSeg3D			Test on Cracks			Test on Thebe		
	DICE	BCD	Hausdorff	DICE	BCD	Hausdorff	DICE	BCD	Hausdorff
Individual Training									
Thebe	0.111±0.036	18.767±18.819	16.095±18.858	0.020±0.008	69.043±15.360	49.012±15.350	0.182±0.019	52.054±7.696	31.615±6.243
FaultSeg3D	0.416±0.059	9.563±9.446	7.191±7.769	0.160±0.046	27.016±7.382	20.638±6.683	0.042±0.008	232.721±28.861	189.939±27.003
Cracks	0.012±0.054	76.904±28.473	57.798±18.930	0.333±0.067	11.330±6.431	7.341±4.732	0.001±0.003	1377.945±143.872	1022.510±114.634
Combined Training									
FaultSeg3D + Cracks	0.662±0.190	6.143±20.421	5.282±18.295	0.333±0.048	15.436±5.254	11.597±4.836	0.001±0.001	659.708±74.985	430.887±64.880
FaultSeg3D + Thebe	0.060±0.031	29.834±20.870	20.151±19.805	0.167±0.033	29.717±8.512	26.136±8.187	0.211±0.024	52.952±10.802	43.348±10.516
Cracks + Thebe	0.038±0.3375	34.183±28.569	22.751±23.675	0.32±0.067	13.797±6.2072	8.2964±4.64058	0.112±0.03	112.354±38.606	60.198±40.66
All	0.337±0.035	28.569±13.036	23.674±11.087	0.306±0.0743	17.7453±21.851	12.005±19.724	0.144±0.029	75.877±37.191	59.039±19.8
Fine-Tuning									
Cracks → FaultSeg3D	0.667±0.171	4.994±16.049	3.821±10.475	0.028±0.009	73.433±13.961	45.378±13.263	0.027±0.003	165.315±10.283	99.996±7.698
Cracks → Thebe	0.099±0.036	21.959±13.845	15.771±10.753	0.159±0.028	26.070±7.107	20.929±6.552	0.181±0.014	53.808±10.361	42.169±12.450
FaultSeg3D → Cracks	0.082±0.080	136.293±151.136	134.095±151.213	0.375±0.059	8.806±3.728	5.577±2.71	0.019±0.005	213.695±20.154	147.213±12.756
FaultSeg3D → Thebe	0.075±0.082	93.488±66.848	84.420±61.439	0.135±0.023	28.701±7.022	23.368±7.111	0.158±0.014	78.683±35.415	51.649±30.973
Thebe → Cracks	0.019±0.027	56.145±34.593	42.899±34.785	0.317±0.047	10.896±3.127	6.656±2.500	0.019±0.005	161.131±14.429	88.344±9.217
Thebe → FaultSeg3D	0.526±0.203	9.319±22.281	8.182±21.079	0.053±0.012	38.141±7.286	34.319±7.233	0.037±0.003	134.522±7.354	122.936±7.078

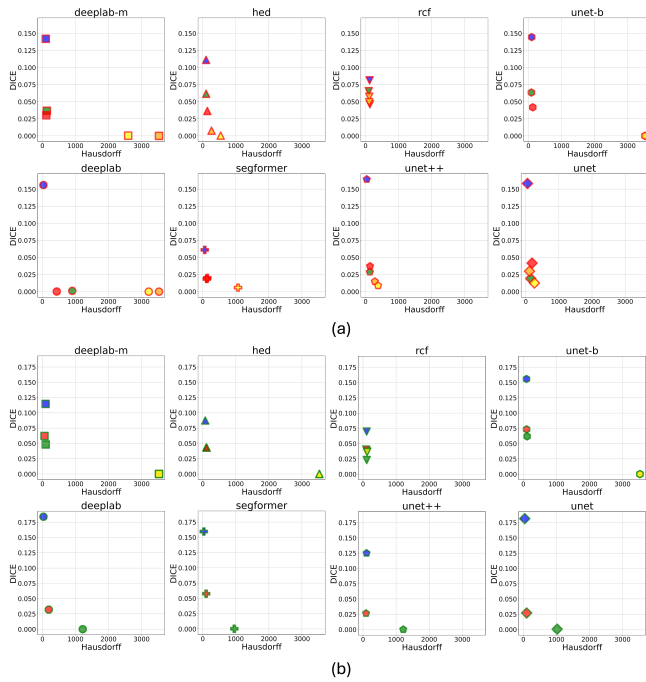


FIGURE 13: Individual models tested on Thebe. (a) Models pre-trained on the FaultSeg3D data, and fine-tuned on different data. (b) Models pre-trained on the CRACKS data, and fine-tuned on different data.

1) Window Size and Loss Function

We evaluate the unet model with a ResNet50 backbone using Dice and Binary Cross-Entropy (BCE) losses, as well as across different window sizes: 96, 128, 256 and 512, or up to the size allowed by the original sections in each dataset. The results for these experiments are shown in Fig. 15, where bigger markers correspond to bigger patch sizes. We can see that when using Dice as a loss, models benefit from having

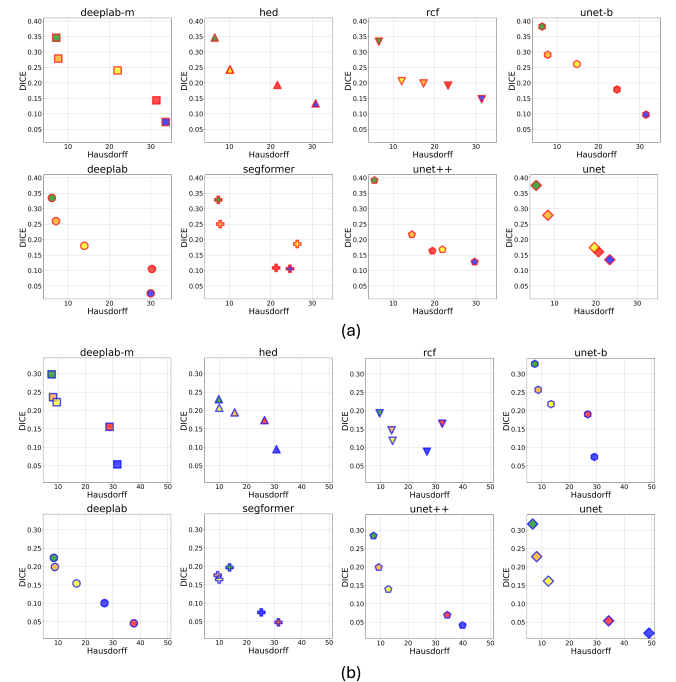


FIGURE 14: Individual models tested on CRACKS. (a) Models pre-trained on the FaultSeg3D data, and fine-tuned on different data. (b) Models pre-trained on the Thebe data, and fine-tuned on different data.

access to larger window sizes, while the same does not hold when using the BCE loss. This discrepancy is due to the class imbalance nature of the fault delineation task: BCE tends to work best when foreground and background are balanced but fails otherwise, and Dice is generally designed for class-imbalanced scenarios [116]. In this context, using smaller patches is equivalent to 'zooming into' the small fault regions and therefore reducing the class imbalance, thus improving

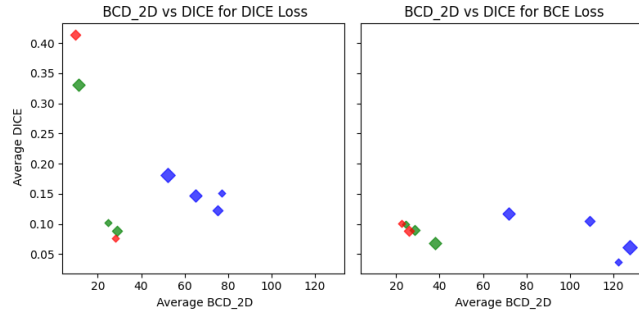


FIGURE 15: Behavior of DICE and BCE losses under different window sizes

BCE performance. Overall, this further validates our choice of using the Dice loss on our benchmarking experiments.

2) Model Nuances in Fault Delineation

We also qualitatively observe that each of the evaluated models presents different nuances in the structure of their fault predictions, irrespective of the pretraining or finetuning strategy used, many of which can be observed in Figs. 19 and 20. For example, *deeplab* tends to produce irregular, stair-like faults, while *segformer* produces thicker, blob-like faults. *unet* architectures in general tend to produce thinner faults, with *unet++* generating more fragmented ones. These architectural signatures are consistent across training setups and highlight the influence model design choices inherently have in shaping the morphology of predicted faults, which is an important consideration when selecting models for downstream tasks or when interpreting evaluation results beyond numerical metrics.

C. METRIC ROBUSTNESS AND OBSERVABILITY

Due to the high correlation among adjacent sections in a seismic volume, deep learning models tend to generate consistent patterns that vary minimally between neighboring sections. Evaluation metrics respond differently to these subtle variations; some metrics heavily penalize these deviations, while others are more tolerant. The effects of structural variations in fault predictions on the evaluation metrics are investigated.

1) Sensitivity to Visual Structure

Distance-based metrics are generally more tolerant to the structure of the predicted fault. This behavior is illustrated in Fig. ???. Where Fig. ??? represents the ground truth, while ??? and ??? show the predictions of two different models. Although the prediction in Fig. ??? appears structurally closer to the ground truth, it receives significantly worse BCD and Hausdorff scores compared to the prediction in Fig. ???. Since distance-based metrics do not heavily weigh continuity, the inclusion of a few extra pixels around the fault can improve the BCD score even if those pixels lack proper structural alignment. Notably, these patterns are not anomalies, different models often generate such consistent

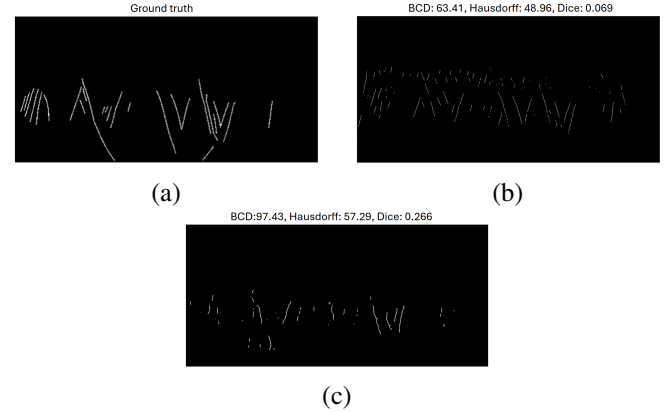


FIGURE 16: Example of the structure tolerance in distance-based metrics. (a) shows the ground truth fault annotations. (b) and (c) show predictions from two different models. While (b) appears structurally closer to the ground truth, it receives a significantly worse BCD and Hausdorff but a better Dice score.

outputs. Consequently, numerical metrics can be misleading and may display discrepancies between one another.

2) Fault Sparsity

Another issue with distance-based metrics is that they are designed to measure the quality of a single continuous object in the image, whereas faults can consist of multiple sparse objects. This makes distance-based metrics very sensitive to both the number of faults present in the ground truth and their sparsity. We showcase this issue in Fig. 17, where we consider two cases: one with a few faults and another with many faults. Noise is added to both images, and each is compared against its original version. The case with fewer faults contains many outliers compared to the case with many faults, since the added noise often lies far from any existing fault. As demonstrated in Fig. 4, because BCD is bidirectional, it accounts for each added noise pixel by searching for its closest existing fault. Therefore, having fewer faults results in a much worse BCD score. DICE, while also penalizing noise, is more stable across different sparsity levels.

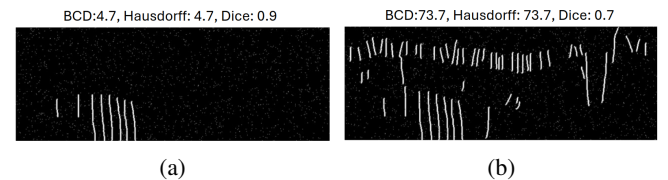
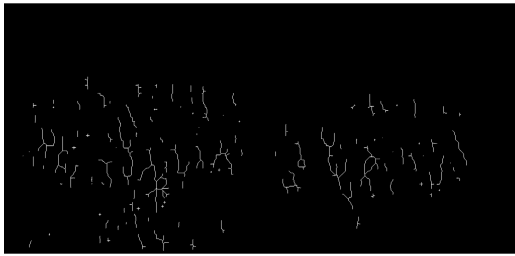


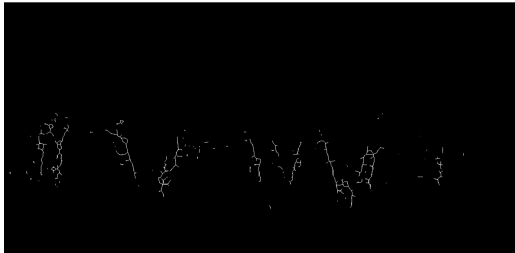
FIGURE 17: Sensitivity of distance-based metrics to fault density: Sections with many (a) vs. few faults (b) are evaluated under identical noise. Despite equal noise levels, (b) is penalized more by distance-based metrics, while Dice remains stable.



(a) Ground Truth



(b) BCD:115.43, Hausdorff: 72.5, Dice: 0.1342



(c) BCD:40.782, Hausdorff: 29.0, Dice: 0.1325

FIGURE 18: (a) Ground truth fault annotations. (b) and (c) display predictions from two different models. Although the prediction in (c) appears visually more aligned with the ground truth than (b), it receives a slightly worse Dice score but substantially better BCD and Hausdorff distance

3) Contradictory Scores and Human Judgement

Although pixel-based metrics are more stable, they remain sensitive to slight pixel shifts. In Fig. 18, we show examples corresponding to two different models. The prediction in Fig. 18c looks visually closer to the ground truth, but receives a worse Dice score (0.1325 vs. 0.13421) and significantly better BCD and Hausdorff (40.782 vs. 115.436 and 29.0 vs 72.5). Since the faults in both predictions are poorly structured and spatially misaligned, the Dice coefficient (being overlap-based) penalizes them similarly. In contrast, distance-based metrics such as BCD and Hausdorff distances are more sensitive to the spatial coherence of the predicted faults, hence, they are more tolerant to the structure of the faults. These contradictions imply that some metrics may conflict with visual intuition or downstream utility, and point to the need for context-aware metric selection frameworks.

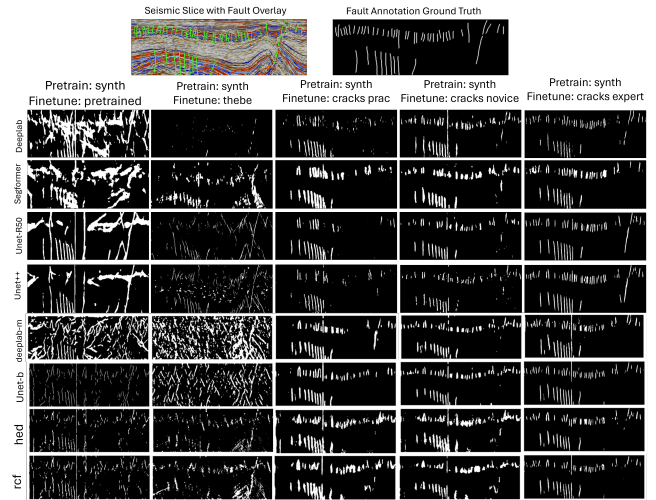


FIGURE 19: Predictions of the models pretrained on FaultSeg3D tested CRACKS

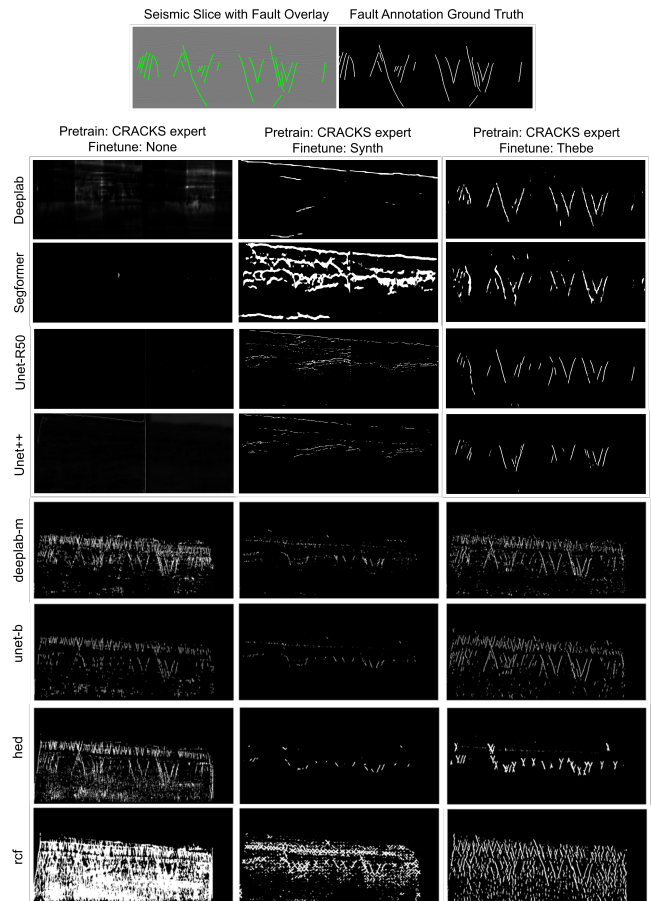


FIGURE 20: Predictions of the models pretrained on CRACKS tested Thebe

TABLE 2: Key observations

Topic	Key Findings
Distributional shift among seismic data	The intensity standard deviation of the synthetic FaultSeg3D data is similar to that of CRACKS, while both are very different from Thebe's. This can be attributed to the discrepancy of seismic features across datasets.
Relationship between CRACKS and FaultSeg3D	Both CRACKS and FaultSeg3D data benefit from pretraining on the other, outperforming models trained from scratch in either.
Thebe vs. others	Thebe does not benefit significantly from pretraining on other data; training from scratch performs best due to distributional shifts.
Model size relationship with pretraining	Larger models like segformer and unet (ResNet50) perform well when pretrained on other datasets and finetuned on FaultSeg3D. Smaller models like rcf and hed degrade in performance with pretraining, indicating a lack of transfer capacity.
Fault density	FaultSeg3D and CRACKS have dense faults; Thebe faults are sparse, affecting model prediction density.
Metric structural biases	Dice penalizes misshaped faults more, while Hausdorff/BCD may still give high scores due to proximity.
Metric sparsity biases	Fewer faults lead to harsher penalty in distance metrics; dense faults often score better.
deeplab behavior	Produces jagged or stair-like faults.
segformer behavior	Tends to generate thick, blob-like faults.
UNET/unet++ behavior	UNET creates thin faults; UNet++ tends to produce fragmented ones.
hed/rcf behavior	Less adaptable to Thebe due to fault density mismatch; outputs noisy, distorted shapes.
Joint CRACKS-FaultSeg3D	Combining CRACKS and FaultSeg3D data leads to synergistic features and better results.
Joint training with Thebe	Adding Thebe acts as a regularizer: performance drops on original domains but improves generalization.

VI. CONCLUSION

In this work, we present the first large-scale benchmarking study of machine learning models for seismic fault delineation under domain shift. By systematically training and evaluating over 200 models across three diverse seismic datasets, we provide a comprehensive analysis of generalization, transferability, and evaluation challenges in seismic segmentation. Our results reveal the fragility of fine-tuning strategies when faced with shifts in data distribution, the emergence of catastrophic forgetting when moving across domains, and the sensitivity of model behavior to architecture and pretraining alignment. We also highlight the limitations of standard evaluation metrics, which often fail to capture geological plausibility, and we advocate for the development of more nuanced frameworks that account for expert ambiguity and structural realism. Collectively, these findings establish a robust empirical foundation for understanding the tradeoffs in current seismic ML workflows and offer practical guidance to researchers and practitioners seeking to build models that are not only accurate but also transferable, interpretable, and aligned with real-world exploration needs.

ACKNOWLEDGMENT

This work is supported by ML4Seismic Industry Partners at the Georgia Institute of Technology.

REFERENCES

- [1] Xinming Wu, Luming Liang, Yunzhi Shi, and Sergey Fomel, "FaultSeg3D: using synthetic datasets to train an end-to-end convolutional neural network for 3D seismic fault segmentation," *GEOPHYSICS*, vol. 84, no. 3, pp. IM35–IM45, 2019.
- [2] Prithwiji Chowdhury, Ahmad Mustafa, Mohit Prabhushankar, and Ghasan AlRegib, "A unified framework for evaluating robustness of machine learning interpretability for prospect risking," *Geophysics*, vol. 90, no. 3, pp. 1–53, 2025.
- [3] Yehuda Ben-Zion, "Collective behavior of earthquakes and faults: Continuum-discrete transitions, progressive evolutionary changes, and different dynamic regimes," *Reviews of Geophysics*, vol. 46, no. 4, 2008.
- [4] Hiroo Kanamori, "72 - earthquake prediction: An overview," in *International Handbook of Earthquake and Engineering Seismology*, Part B, William H.K. Lee, Hiroo Kanamori, Paul C. Jennings, and Carl Kisslinger, Eds., vol. 81 of *International Geophysics*, pp. 1205–1216. Academic Press, 2003.
- [5] Zeren Zhang, Ran Chen, and Jinwen Ma, "Improving seismic fault recognition with self-supervised pre-training: A study of 3d transformer-based with multi-scale decoding and fusion," *Remote Sensing*, vol. 16, no. 5, 2024.
- [6] Ran Chen, Zeren Zhang, and Jinwen Ma, "Seismic fault sam: Adapting sam with lightweight modules and 2.5d strategy for fault detection," 10 2024, pp. 436–441.
- [7] M Quamer Nasim, Tannistha Maiti, Ayush Srivastava, Tarry Singh, and Jie Mei, "Seismic facies analysis: A deep domain adaptation approach," *arXiv preprint arXiv:2011.10510*, 2020.
- [8] Xiao Li, Kewen Li, Zhifeng Xu, Zongchao Huang, and Yimin Dou, "Fault-seg-net: A method for seismic fault segmentation based on multi-scale feature fusion with imbalanced classification," *Computers and Geotechnics*, vol. 158, pp. 105412, 2023.
- [9] Yazeed Alaudah, Motaz Alfarraj, and Ghasan AlRegib, "Structure label prediction using similarity-based retrieval and weakly supervised label mapping," *Geophysics*, vol. 84, no. 1, pp. V67–V79, 2018.
- [10] Yazeed Alaudah, Patrycja Michałowicz, Motaz Alfarraj, and Ghasan

- AIRegib, "A machine-learning benchmark for facies classification," *Interpretation*, vol. 7, no. 3, pp. SE175–SE187, 2019.
- [11] Yu An, Jiulin Guo, Qing Ye, Conrad Childs, John Walsh, and Ruihai Dong, "A gigabyte interpreted seismic dataset for automatic fault recognition," *Data in Brief*, vol. 37, pp. 107219, 2021.
 - [12] Ryan Benkert, Mohit Prabhushankar, and Ghassan AIRegib, "Reliable uncertainty estimation for seismic interpretation with prediction switches," in *Second International Meeting for Applied Geoscience & Energy. Society of Exploration Geophysicists and American Association of Petroleum ...*, 2022, pp. 1740–1744.
 - [13] Ryan Benkert, Mohit Prabhushankar, and Ghassan AIRegib, "What samples must seismic interpreters label for efficient machine learning?," in *Third International Meeting for Applied Geoscience & Energy. Society of Exploration Geophysicists and American Association of Petroleum ...*, 2023, pp. 1004–1009.
 - [14] Ahmad Mustafa and Ghassan AIRegib, "Man-recon: Manifold learning for reconstruction with deep autoencoder for smart seismic interpretation," in *2021 IEEE International Conference on Image Processing (ICIP)*. IEEE, 2021, pp. 2953–2957.
 - [15] Zhen Wang and Ghassan AIRegib, "Interactive fault extraction in 3-d seismic data using the hough transform and tracking vectors," *IEEE Transactions on Computational Imaging*, vol. 3, no. 1, pp. 99–109, 2016.
 - [16] Israel Cohen, Nicholas Coult, and Anthony A Vassiliou, "Detection and extraction of fault surfaces in 3d seismic data," *Geophysics*, vol. 71, no. 4, pp. P21–P27, 2006.
 - [17] Andy Roberts, "Curvature attributes and their application to 3 d interpreted horizons," *First break*, vol. 19, no. 2, pp. 85–100, 2001.
 - [18] Haibin Di, Muhammad Amir Shafiq, and Ghassan AIRegib, "Seismic-fault detection based on multiattribute support vector machine analysis," in *SEG International Exposition and Annual Meeting. SEG*, 2017, pp. SEG–2017.
 - [19] Muhammad A Shafiq, Mohit Prabhushankar, Haibin Di, and Ghassan AIRegib, "Towards understanding common features between natural and seismic images," in *SEG International Exposition and Annual Meeting. SEG*, 2018, pp. SEG–2018.
 - [20] Kiran Kokilepersaud, Mohit Prabhushankar, and Ghassan AIRegib, "Volumetric supervised contrastive learning for seismic semantic segmentation," in *Second International Meeting for Applied Geoscience & Energy. Society of Exploration Geophysicists and American Association of Petroleum ...*, 2022, pp. 1699–1703.
 - [21] Jorge Quesada, Mohammad Alotaibi, Mohit Prabhushankar, and Ghassan AIRegib, "Pointprompt: A multi-modal prompting dataset for segment anything model," in *Proceedings of the IEEE/CVF Conference on Computer Vision and Pattern Recognition (CVPR) Workshops*, June 2024, pp. 1604–1610.
 - [22] Jorge Quesada, Zoe Fowler, Mohammad Alotaibi, Mohit Prabhushankar, and Ghassan AIRegib, "Benchmarking human and automated prompting in the segment anything model," in *2024 IEEE International Conference on Big Data (BigData)*. IEEE, 2024, pp. 1625–1634.
 - [23] James Kirkpatrick, Razvan Pascanu, Neil Rabinowitz, Joel Veness, Guillaume Desjardins, Andrei A Rusu, Kieran Milan, John Quan, Tiago Ramalho, Agnieszka Grabska-Barwinska, et al., "Overcoming catastrophic forgetting in neural networks," *Proceedings of the national academy of sciences*, vol. 114, no. 13, pp. 3521–3526, 2017.
 - [24] Juan Alcalde, Clare E. Bond, Gareth Johnson, Jennifer F. Ellis, and Robert W.H. Butler, "Impact of seismic image quality on fault interpretation uncertainty," *GSA Today*, vol. 27, no. 2, pp. 4–10, 2017.
 - [25] Sébastien Guillon, Frédéric Joncour, Pierre-Emmanuel Barrallon, and Laurent Castanié, "Ground-truth uncertainty-aware metrics for machine learning applications on seismic image interpretation: Application to faults and horizon extraction," *The Leading Edge*, vol. 39, no. 10, pp. 734–741, 2020.
 - [26] M. Sarajärvi, T. Hellem Bo, B. Goleadowski, and M. Nickel, "Robust evaluation of fault prediction results: Machine learning using synthetic seismic," in *First EAGE Digitalization Conference and Exhibition*. 2020, European Association of Geoscientists & Engineers.
 - [27] Jia Deng, Wei Dong, Richard Socher, Li-Jia Li, Kai Li, and Li Fei-Fei, "Imagenet: A large-scale hierarchical image database," in *2009 IEEE conference on computer vision and pattern recognition*. Ieee, 2009, pp. 248–255.
 - [28] Jonathan Long, Evan Shelhamer, and Trevor Darrell, "Fully convolutional networks for semantic segmentation," in *Proceedings of the IEEE conference on computer vision and pattern recognition*, 2015, pp. 3431–3440.
 - [29] Liang-Chieh Chen, George Papandreou, Iasonas Kokkinos, Kevin Murphy, and Alan L Yuille, "DeepLab: Semantic image segmentation with deep convolutional nets, atrous convolution, and fully connected crfs," *IEEE transactions on pattern analysis and machine intelligence*, vol. 40, no. 4, pp. 834–848, 2017.
 - [30] Kiran Kokilepersaud, Yash-Yee Logan, Ryan Benkert, Chen Zhou, Mohit Prabhushankar, Ghassan AIRegib, Enrique Corona, Kunjan Singh, and Mostafa Parchami, "Focal: A cost-aware video dataset for active learning," in *2023 IEEE International Conference on Big Data (BigData)*. IEEE, 2023, pp. 1269–1278.
 - [31] Olaf Ronneberger, Philipp Fischer, and Thomas Brox, "U-net: Convolutional networks for biomedical image segmentation," in *International Conference on Medical image computing and computer-assisted intervention*. Springer, 2015, pp. 234–241.
 - [32] Fabian Isensee, Paul F Jaeger, Simon AA Kohl, Jens Petersen, and Klaus H Maier-Hein, "nnu-net: a self-configuring method for deep learning-based biomedical image segmentation," *Nature methods*, vol. 18, no. 2, pp. 203–211, 2021.
 - [33] Mohit Prabhushankar, Kiran Kokilepersaud, Yash-yee Logan, Stephanie Trejo Corona, Ghassan AIRegib, and Charles Wykoff, "Olives dataset: Ophthalmic labels for investigating visual eye semantics," *Advances in Neural Information Processing Systems*, vol. 35, pp. 9201–9216, 2022.
 - [34] Sergey Ioffe and Christian Szegedy, "Batch normalization: Accelerating deep network training by reducing internal covariate shift," in *International conference on machine learning*. pmlr, 2015, pp. 448–456.
 - [35] Dmitry Ulyanov, Andrea Vedaldi, and Victor Lempitsky, "Instance normalization: The missing ingredient for fast stylization," *arXiv preprint arXiv:1607.08022*, 2016.
 - [36] Mohit Prabhushankar, Dogancan Temel, and Ghassan AIRegib, "Generating adaptive and robust filter sets using an unsupervised learning framework," in *2017 IEEE International Conference on Image Processing (ICIP)*. IEEE, 2017, pp. 3041–3045.
 - [37] Connor Shorten and Taghi M Khoshgoftaar, "A survey on image data augmentation for deep learning," *Journal of big data*, vol. 6, no. 1, pp. 1–48, 2019.
 - [38] Jason Wang, Luis Perez, et al., "The effectiveness of data augmentation in image classification using deep learning," *Convolutional Neural Networks Vis. Recognit*, vol. 11, no. 2017, pp. 1–8, 2017.
 - [39] Enze Xie, Wenhai Wang, Zhiding Yu, Anima Anandkumar, Jose M Alvarez, and Ping Luo, "Segformer: Simple and efficient design for semantic segmentation with transformers," in *Advances in Neural Information Processing Systems*, 2021, vol. 34, pp. 12077–12090.
 - [40] David R Cox, "The regression analysis of binary sequences," *Journal of the Royal Statistical Society Series B: Statistical Methodology*, vol. 20, no. 2, pp. 215–232, 1958.
 - [41] Fausto Milletari, Nassir Navab, and Seyed-Ahmad Ahmadi, "V-net: Fully convolutional neural networks for volumetric medical image segmentation," in *2016 fourth international conference on 3D vision (3DV)*. Ieee, 2016, pp. 565–571.
 - [42] Saad Wazir and Muhammad Moazam Fraz, "Histoseg: Quick attention with multi-loss function for multi-structure segmentation in digital histology images," in *2022 12th International Conference on Pattern Recognition Systems (ICPRS)*. IEEE, 2022, pp. 1–7.
 - [43] Shaohuan Zu, Penghui Zhao, Chaofan Ke, and Cao Junxing, "Resaccunet: An improved transformer unet model for 3d seismic fault detection," *Journal of Geophysical Research: Machine Learning and Computation*, vol. 1, no. 3, pp. e2024JH000232, 2024, e2024JH000232.
 - [44] Haibin Di, Dengliang Gao, and Ghassan AIRegib, "Developing a seismic texture analysis neural network for machine-aided seismic pattern recognition and classification," *Geophysical Journal International*, vol. 218, no. 2, pp. 1262–1275, 2019.
 - [45] Haibin Di, Mohammad Amir Shafiq, Zhen Wang, and Ghassan AIRegib, "Improving seismic fault detection by super-attribute-based classification," *Interpretation*, vol. 7, no. 3, pp. SE251–SE267, 2019.
 - [46] Haibin Di and Ghassan AIRegib, "Semi-automatic fault/fracture interpretation based on seismic geometry analysis," *Geophysical Prospecting*, vol. 67, no. 5, pp. 1379–1391, 2019.
 - [47] Yimin Dou, Kewen Li, Jianbing Zhu, Timing Li, Shaoquan Tan, and Zongchao Huang, "Md loss: Efficient training of 3-d seismic fault segmentation network under sparse labels by weakening anomaly annotation," *IEEE Transactions on Geoscience and Remote Sensing*, vol. 60, pp. 1–14, 2022.

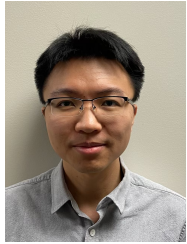
- [48] Ryan Benkert, Mohit Prabhushankar, and Ghassan AlRegib, "Effective data selection for seismic interpretation through disagreement," *IEEE Transactions on Geoscience and Remote Sensing*, 2024.
- [49] Ahmad Mustafa and Ghassan AlRegib, "Active learning with deep autoencoders for seismic facies interpretation," *Geophysics*, vol. 88, no. 4, pp. IM77–IM86, 2023.
- [50] Ahmad Mustafa, Reza Rastegar, Tim Brown, Gregory Nunes, Daniel DeLilla, and Ghassan AlRegib, "Visual attention guided learning with incomplete labels for seismic fault interpretation," *IEEE Transactions on Geoscience and Remote Sensing*, 2024.
- [51] Ian Goodfellow, Yoshua Bengio, Aaron Courville, and Yoshua Bengio, *Deep learning*, vol. 1, MIT press Cambridge, 2016.
- [52] Ryan Benkert, Oluwaseun Joseph Aribido, and Ghassan AlRegib, "Example forgetting: A novel approach to explain and interpret deep neural networks in seismic interpretation," *IEEE Transactions on Geoscience and Remote Sensing*, vol. 60, pp. 1–12, 2022.
- [53] Ahmad Mustafa, Motaz Alfarraj, and Ghassan AlRegib, "Joint learning for spatial context-based seismic inversion of multiple data sets for improved generalizability and robustness," *Geophysics*, vol. 86, no. 4, pp. O37–O48, 2021.
- [54] Antonio Torralba and Alexei A Efros, "Unbiased look at dataset bias," in *CVPR 2011*. IEEE, 2011, pp. 1521–1528.
- [55] D. Temel, G. Kwon, M. Prabhushankar, and G. AlRegib, "Cure-ts: Challenging unreal and real environments for traffic sign recognition," in *Neural Information Processing Systems (NIPS) Workshop on Machine Learning for Intelligent Transportation Systems (MLITS)*, December 2017.
- [56] Dogancan Temel, Jinsol Lee, and Ghassan AlRegib, "Cure-or: Challenging unreal and real environments for object recognition," in *2018 17th IEEE international conference on machine learning and applications (ICMLA)*. IEEE, 2018, pp. 137–144.
- [57] Dogancan Temel, Min-Hung Chen, and Ghassan AlRegib, "Traffic sign detection under challenging conditions: A deeper look into performance variations and spectral characteristics," *IEEE Transactions on Intelligent Transportation Systems*, vol. 21, no. 9, pp. 3663–3673, 2019.
- [58] Mohit Prabhushankar and Ghassan AlRegib, "Introspective learning: A two-stage approach for inference in neural networks," *Advances in Neural Information Processing Systems*, vol. 35, pp. 12126–12140, 2022.
- [59] Yaroslav Ganin, Evgeniya Ustinova, Hana Ajakan, Pascal Germain, Hugo Larochelle, François Laviolette, Mario March, and Victor Lempitsky, "Domain-adversarial training of neural networks," *Journal of machine learning research*, vol. 17, no. 59, pp. 1–35, 2016.
- [60] Min-Hung Chen, Zsolt Kira, Ghassan AlRegib, Jaekwon Yoo, Ruxin Chen, and Jian Zheng, "Temporal attentive alignment for large-scale video domain adaptation," in *Proceedings of the IEEE/CVF international conference on computer vision*, 2019, pp. 6321–6330.
- [61] Santisudha Panigrahi, Anuja Nanda, and Tripti Swarnkar, "A survey on transfer learning," in *Intelligent and Cloud Computing: Proceedings of ICICC 2019*, Volume 1, pp. 781–789. Springer, 2020.
- [62] Jason Yosinski, Jeff Clune, Yoshua Bengio, and Hod Lipson, "How transferable are features in deep neural networks?," *Advances in neural information processing systems*, vol. 27, 2014.
- [63] Maurizio Ercoli, Filippo Carboni, Assel Akimbekova, Ramon Bertran Carbonell, and Massimiliano Rinaldo Barchi, "Evidencing subtle faults in deep seismic reflection profiles: Data pre-conditioning and seismic attribute analysis of the legacy crop-04 profile," *Frontiers in Earth Science*, vol. 11, pp. 1119554, 2023.
- [64] Baochen Sun and Kate Saenko, "Deep coral: Correlation alignment for deep domain adaptation," in *Computer vision–ECCV 2016 workshops: Amsterdam, the Netherlands, October 8–10 and 15–16, 2016, proceedings, part III* 14. Springer, 2016, pp. 443–450.
- [65] Yi-Hsuan Tsai, Wei-Chih Hung, Samuel Schuster, Kihyuk Sohn, Ming-Hsuan Yang, and Manmohan Chandraker, "Learning to adapt structured output space for semantic segmentation," in *Proceedings of the IEEE conference on computer vision and pattern recognition*, 2018, pp. 7472–7481.
- [66] Haiwen Du, Yu An, Qing Ye, Jiulin Guo, Lu Liu, Dongjie Zhu, Conrad Childs, John Walsh, and Ruihai Dong, "Disentangling noise patterns from seismic images: Noise reduction and style transfer," *IEEE Transactions on Geoscience and Remote Sensing*, vol. 60, pp. 1–14, 2022.
- [67] Shenghou Wang, Xu Si, Zhongxian Cai, and Yatong Cui, "Structural augmentation in seismic data for fault prediction," *Applied Sciences*, vol. 12, no. 19, pp. 9796, 2022.
- [68] Kaiming He, Xiangyu Zhang, Shaoqing Ren, and Jian Sun, "Deep residual learning for image recognition," in *Proceedings of the IEEE conference on computer vision and pattern recognition*, 2016, pp. 770–778.
- [69] Karen Simonyan and Andrew Zisserman, "Very deep convolutional networks for large-scale image recognition," *arXiv preprint arXiv:1409.1556*, 2014.
- [70] Philipp Krähenbühl and Vladlen Koltun, "Efficient inference in fully connected crfs with gaussian edge potentials," *Advances in neural information processing systems*, vol. 24, 2011.
- [71] Tobias Pohlen, Alexander Hermans, Markus Mathias, and Bastian Leibe, "Full-resolution residual networks for semantic segmentation in street scenes," in *Proceedings of the IEEE conference on computer vision and pattern recognition*, 2017, pp. 4151–4160.
- [72] Orhun Utku Aydın, Abdel Aziz Taha, Adam Hilbert, Ahmed A. Khalil, Ivana Galinovic, Jochen B. Fiebach, Dietmar Frey, and Vince Istvan Madai, "On the usage of average hausdorff distance for segmentation performance assessment: Hidden bias when used for ranking," 2020.
- [73] M.-P. Dubuisson and A.K. Jain, "A modified hausdorff distance for object matching," in *Proceedings of 12th International Conference on Pattern Recognition*, 1994, vol. 1, pp. 566–568 vol.1.
- [74] You Li, Xinming Wu, Zhenyu Zhu, Jicai Ding, and Qingzhen Wang, "Faultseg3d plus: A comprehensive study on evaluating and improving cnn-based seismic fault segmentation," *GEOPHYSICS*, vol. 89, no. 5, pp. N77–N91, 2024.
- [75] Yu An, Haiwen Du, Siteng Ma, Yingjie Niu, Dairui Liu, Jing Wang, Yuhuan Du, Conrad Childs, John Walsh, and Ruihai Dong, "Current state and future directions for deep learning based automatic seismic fault interpretation: A systematic review," *Earth-Science Reviews*, vol. 243, pp. 104509, 2023.
- [76] Yazeed Alaudah and Ghassan AlRegib, "A curvelet-based distance measure for seismic images," in *2015 IEEE International Conference on Image Processing (ICIP)*. IEEE, 2015, pp. 4200–4204.
- [77] Motaz Alfarraj, Yazeed Alaudah, Zhiling Long, and Ghassan AlRegib, "Multiresolution analysis and learning for computational seismic interpretation," *The Leading Edge*, vol. 37, no. 6, pp. 443–450, 2018.
- [78] Zhiling Long, Yazeed Alaudah, Muhammad Ali Qureshi, Yuting Hu, Zhen Wang, Motaz Alfarraj, Ghassan AlRegib, Asjad Amin, Mohamed Deriche, Suhail Al-Dharrab, et al., "A comparative study of texture attributes for characterizing subsurface structures in seismic volumes," *Interpretation*, vol. 6, no. 4, pp. T1055–T1066, 2018.
- [79] Zhiling Long*, Yazeed Alaudah, Muhammad Ali Qureshi, Motaz Al Farraj, Zhen Wang, Asjad Amin, Mohamed Deriche, and Ghassan AlRegib, "Characterization of migrated seismic volumes using texture attributes: a comparative study," in *SEG Technical Program Expanded Abstracts 2015*, pp. 1744–1748. Society of Exploration Geophysicists, 2015.
- [80] Yazeed Alaudah, Shan Gao, and Ghassan AlRegib, "Learning to label seismic structures with deconvolution networks and weak labels," in *SEG international exposition and annual meeting. SEG*, 2018, pp. SEG–2018.
- [81] Oluwaseun Joseph Aribido, Ghassan AlRegib, and Mohamed Deriche, "Self-supervised annotation of seismic images using latent space factorization," in *2020 IEEE International Conference on Image Processing (ICIP)*. IEEE, 2020, pp. 2421–2425.
- [82] Oluwaseun Joseph Aribido, Ghassan AlRegib, and Yazeed Alaudah, "Self-supervised delineation of geologic structures using orthogonal latent space projection," *Geophysics*, vol. 86, no. 6, pp. V497–V508, 2021.
- [83] Haibin Di, Zhen Wang, and Ghassan AlRegib, "Seismic fault detection from post-stack amplitude by convolutional neural networks," in *80th EAGE Conference and Exhibition 2018. European Association of Geoscientists & Engineers*, 2018, vol. 2018, pp. 1–5.
- [84] Yu An, Jiulin Guo, Qing Ye, Conrad Childs, John Walsh, and Ruihai Dong, "Deep convolutional neural network for automatic fault recognition from 3d seismic datasets," *Computers & Geosciences*, vol. 153, pp. 104776, 2021.
- [85] Yu An, Qing Ye, Jiulin Guo, and Ruihai Dong, "Overlap training to mitigate inconsistencies caused by image tiling in cnns," in *International Conference on Innovative Techniques and Applications of Artificial Intelligence*. Springer, 2020, pp. 35–48.
- [86] Mohit Prabhushankar, Kiran Kokilepersaud, Jorge Quesada, Yavuz Yarci, Chen Zhou, Mohammad Alotaibi, Ghassan AlRegib, Ahmad Mustafa, and Yusufjon Kumakov, "Cracks: Crowdsourcing resources for analysis and categorization of key subsurface faults," *arXiv preprint arXiv:2408.11185*, 2024.

- [87] Zhengfa Bi, Xinming Wu, Zhicheng Geng, and Haishan Li, "Deep relative geologic time: a deep learning method for simultaneously interpreting 3-d seismic horizons and faults," *Journal of Geophysical Research: Solid Earth*, vol. 126, no. 9, pp. e2021JB021882, 2021.
- [88] Lei Lin, Zhi Zhong, Zhongxian Cai, Alexander Y Sun, and ChengLong Li, "Automatic geologic fault identification from seismic data using 2.5 d channel attention u-net," *Geophysics*, vol. 87, no. 4, pp. IM111–IM124, 2022.
- [89] Axelle Pochet, Pedro HB Diniz, H  lio Lopes, and Marcelo Gattass, "Seismic fault detection using convolutional neural networks trained on synthetic poststacked amplitude maps," *IEEE Geoscience and Remote Sensing Letters*, vol. 16, no. 3, pp. 352–356, 2018.
- [90] dGB Earth Sciences, "The netherlands offshore, the north sea, f3 block—complete," 1987.
- [91] Ahmad Mustafa, Klaas Koster, and Ghassan AlRegib, "Explainable machine learning for hydrocarbon prospect risking," *Geophysics*, vol. 89, no. 1, pp. WA13–WA24, 2024.
- [92] Chen Zhou, Mohit Prabhushankar, and Ghassan AlRegib, "Perceptual quality-based model training under annotator label uncertainty," in *SEG International Exposition and Annual Meeting*. SEG, 2023, pp. SEG–2023.
- [93] Prithwiji Chowdhury, Ahmad Mustafa, Mohit Prabhushankar, and Ghassan AlRegib, "Counterfactual uncertainty for high dimensional tabular dataset," in *SEG International Exposition and Annual Meeting*. SEG, 2023, pp. SEG–2023.
- [94] Muhammad Amir Shafiq, Zhiling Long, Haibin Di, and Ghassan AlRegib, "A novel attention model for salient structure detection in seismic volumes," *arXiv preprint arXiv:2201.06174*, 2022.
- [95] Naveed Iqbal, Mohamed Deriche, Ghassan AlRegib, and Sikandar Khan, "Blind curvelet-based denoising of seismic surveys in coherent and incoherent noise environments," *Arabian Journal for Science and Engineering*, vol. 48, no. 8, pp. 10925–10935, 2023.
- [96] Ahmad Mustafa and Ghassan AlRegib, "A comparative study of transfer learning methodologies and causality for seismic inversion with temporal convolutional networks," in *SEG International Exposition and Annual Meeting*. SEG, 2021, p. D011S067R001.
- [97] Ryan Benkert, Oluwaseun Joseph Aribido, and Ghassan AlRegib, "Explaining deep models through forgettable learning dynamics," in *2021 IEEE International Conference on Image Processing (ICIP)*. IEEE, 2021, pp. 3692–3696.
- [98] Ryan Benkert, Oluwaseun Joseph Aribido, and Ghassan AlRegib, "Explainable seismic neural networks using learning statistics," in *First International Meeting for Applied Geoscience & Energy*. Society of Exploration Geophysicists, 2021, pp. 1425–1429.
- [99] Ahmad Mustafa, Motaz Alfarraj, and Ghassan AlRegib, "Spatiotemporal modeling of seismic images for acoustic impedance estimation," in *SEG International Exposition and Annual Meeting*. SEG, 2020, p. D041S101R005.
- [100] Ahmad Mustafa and Ghassan AlRegib, "Joint learning for seismic inversion: An acoustic impedance estimation case study," in *SEG Technical Program Expanded Abstracts 2020*, pp. 1686–1690. Society of Exploration Geophysicists, 2020.
- [101] Moamen Soliman, Charles Lehman, and Ghassan AlRegib, "S 6: semi-supervised self-supervised semantic segmentation," in *2020 IEEE International Conference on Image Processing (ICIP)*. IEEE, 2020, pp. 1861–1865.
- [102] Motaz Alfarraj and Ghassan AlRegib, "Semisupervised sequence modeling for elastic impedance inversion," *Interpretation*, vol. 7, no. 3, pp. SE237–SE249, 2019.
- [103] Haibin Di and Ghassan AlRegib, "Reflector dip estimates based on seismic waveform curvature/flexure analysis," *Interpretation*, vol. 7, no. 2, pp. SC1–SC9, 2019.
- [104] Yazeed Alaudah, Moamen Soliman, and Ghassan AlRegib, "Facies classification with weak and strong supervision: A comparative study," in *SEG International Exposition and Annual Meeting*. SEG, 2019, p. D033S037R004.
- [105] Ahmad Mustafa, Motaz Alfarraj, and Ghassan AlRegib, "Estimation of acoustic impedance from seismic data using temporal convolutional network," in *SEG technical program expanded abstracts 2019*, pp. 2554–2558. Society of Exploration Geophysicists, 2019.
- [106] Motaz Alfarraj and Ghassan AlRegib, "Semi-supervised learning for acoustic impedance inversion," in *SEG technical program expanded abstracts 2019*, pp. 2298–2302. Society of Exploration Geophysicists, 2019.
- [107] Mohammad Afifi Ishak, Md Aminul Islam, Mohamed Ragab Shalaby, and Nurul Hasan, "The application of seismic attributes and wheeler transformations for the geomorphological interpretation of stratigraphic surfaces: a case study of the f3 block, dutch offshore sector, north sea," *Geosciences*, vol. 8, no. 3, pp. 79, 2018.
- [108] Mohammad Reza Safari, Kioumars Taheri, Hosein Hashemi, and Ali Hadadi, "Structural smoothing on mixed instantaneous phase energy for automatic fault and horizon picking: case study on f3 north sea," *Journal of Petroleum Exploration and Production Technology*, vol. 13, no. 3, pp. 775–785, 2023.
- [109] Yu An and Ruihai Dong, "Understanding the effect of different prior knowledge on cnn fault interpreter," *IEEE Access*, vol. 11, pp. 15058–15068, 2023.
- [110] Zhiguo Wang, Qiannan Wang, Yang Yang, Naihao Liu, Yumin Chen, and Jinghuai Gao, "Seismic facies segmentation via a segformer-based specific encoder–decoder–hypercolumns scheme," *IEEE Transactions on Geoscience and Remote Sensing*, vol. 61, pp. 1–11, 2023.
- [111] Liang-Chieh Chen, Yukun Zhu, George Papandreou, Florian Schroff, and Hartwig Adam, "Encoder-decoder with atrous separable convolution for semantic image segmentation," in *Proceedings of the European conference on computer vision (ECCV)*, 2018, pp. 801–818.
- [112] Mark Sandler, Andrew Howard, Menglong Zhu, Andrey Zhmoginov, and Liang-Chieh Chen, "Mobilenetv2: Inverted residuals and linear bottlenecks," in *Proceedings of the IEEE conference on computer vision and pattern recognition*, 2018, pp. 4510–4520.
- [113] Saining Xie and Zhuowen Tu, "Holistically-nested edge detection," in *Proceedings of the IEEE international conference on computer vision*, 2015, pp. 1395–1403.
- [114] Yun Liu, Song Cheng, Yunchao Hu, Yandong Wang, Xiang Bai, and Alan L Yuille, "Richer convolutional features for edge detection," in *Proceedings of the IEEE conference on computer vision and pattern recognition*, 2017, pp. 3000–3009.
- [115] Zongwei Zhou, Md Mahfuzur Rahman Siddiquee, Nima Tajbakhsh, and Jianming Liang, "Unet++: A nested u-net architecture for medical image segmentation," in *Deep learning in medical image analysis and multimodal learning for clinical decision support*. Springer, 2018, pp. 3–11.
- [116] Carole H Sudre, Wenqi Li, Tom Vercauteren, Sebastien Ourselin, and M Jorge Cardoso, "Generalised dice overlap as a deep learning loss function for highly unbalanced segmentations," in *Deep Learning in Medical Image Analysis and Multimodal Learning for Clinical Decision Support: Third International Workshop, DLMIA 2017, and 7th International Workshop, ML-CDS 2017, Held in Conjunction with MICCAI 2017, Qu  bec City, QC, Canada, September 14, Proceedings 3*. Springer, 2017, pp. 240–248.



vision.

JORGE QUESADA received his B.E. and M.S. degrees from the Pontifical Catholic University of Peru. He joined the Georgia Institute of Technology as a Machine Learning PhD student in the department of Electrical and Computer Engineering in 2021, where he is now part of the Omni Lab for Intelligent Visual Engineering and Science (OLIVES). He is interested in leveraging machine learning and image processing tools to study the mechanisms underlying computer and biological



interpretation.

CHEN ZHOU is a Ph.D. student in the School of Electrical and Computer Engineering at the Georgia Institute of Technology. He is currently a Graduate Research Assistant in the Omni Lab for Intelligent Visual Engineering and Science (OLIVES). He is working in the fields of machine learning, and image and video processing. His research interests include trajectory prediction and learning from label disagreement for the applications of autonomous vehicle, and seismic



YUSUFJON KUMAKOV is currently serving as an Assistant Lecturer at Tashkent State Technical University. He earned his Master's degree in Petroleum Engineering from the Polytechnic University of Turin, Italy. His primary research interests lie in the application of machine learning techniques to geophysics, with a focus on seismic imaging and signal processing.



and machine learning with applications to geophysics. He is an IEEE Student Member and a published author, with several works presented at the IMAGE conference and published in the GEOPHYSICS journal.

PRITHWIJIT CHOWDHURY received his B.Tech. degree from KIIT University, India, in 2020. He joined the Georgia Institute of Technology as an M.S. student in the School of Electrical and Computer Engineering in 2021 and is currently pursuing his Ph.D. as a researcher in The Center for Energy and Geo Processing (CeGP) and as a member of the Omni Lab for Intelligent Visual Engineering and Science (OLIVES). His research interests lie in digital signal and image processing



healthcare, and robust and explainable AI. He is the recipient of the Best Paper award at ICIP 2019 and Top Viewed Special Session Paper Award at ICIP 2020. He is the recipient of the ECE Outstanding Graduate Teaching Award, the CSIP Research award, and of the Roger P Webb ECE Graduate Research Assistant Excellence award, all in 2022. He has delivered short courses and tutorials at IEEE IV'23, ICIP'23, BigData'23, WACV'24 and AAAI'24.

MOHIT PRABHUSHANKAR received his Ph.D. degree in electrical engineering from the Georgia Institute of Technology (Georgia Tech), Atlanta, Georgia, 30332, USA, in 2021. He is currently a Postdoctoral Research Fellow in the School of Electrical and Computer Engineering at the Georgia Institute of Technology in the Omni Lab for Intelligent Visual Engineering and Science (OLIVES). He is working in the fields of image processing, machine learning, active learning,



MOHAMMAD ALOTAIBI is a Ph.D. student in the School of Electrical and Computer Engineering at the Georgia Institute of Technology. He is a Graduate Research Assistant in the Omni Lab for Intelligent Visual Engineering and Science (OLIVES). His research focuses on machine learning and image processing, with particular interest in domain adaptation for seismic and medical imaging applications.



Systems, Medical Imaging, and Subsurface Imaging. The group is interested in advancing the fundamentals as well as the deployment of such systems in real-world scenarios. He has been issued several U.S. patents and invention disclosures. He is a Fellow of the IEEE. Prof. AlRegib is active in the IEEE. He served on the editorial board of several transactions and served as the TPC Chair for ICIP 2020, ICIP 2024, and GlobalSIP 2014. He was area editor for the IEEE Signal Processing Magazine. In 2008, he received the ECE Outstanding Junior Faculty Member Award. In 2017, he received the 2017 Denning Faculty Award for Global Engagement. He received the 2024 ECE Distinguished Faculty Achievement Award at Georgia Tech. He and his students received the Best Paper Award in ICIP 2019 and the 2023 EURASIP Best Paper Award for Image communication Journal. In addition, one of their papers is the best paper runner-up at BigData 2024. In 2024, he co-founded the AI Makerspace at Georgia Tech, where any student and any community member can access and utilize AI regardless of their background.

GHASSAN ALREGIB is currently the John and Marilu McCarty Chair Professor in the School of Electrical and Computer Engineering at the Georgia Institute of Technology. In the Omni Lab for Intelligent Visual Engineering and Science (OLIVES), he and his groupwork on robust and interpretable machine learning algorithms, uncertainty and trust, and human in the loop algorithms. The group has demonstrated their work on a widerange of applications such as Autonomous



prestigious Roger P. Webb ECE GRA Excellence Award in recognition of his research contributions. He has been involved in various teaching and instructional activities in both academic and industrial settings. His teaching services at Georgia Tech earned him several accolades, such as the Outstanding Online Head TA Award, the ECE GTA Excellence Award and the ECE CREATION Award, respectively.

AHMAD MUSTAFA received his PhD in Electrical and Computer Engineering at the Georgia Institute of Technology. His research interests span deep learning, computer vision, and signal processing for medical and geophysical applications. He served as a Staff Scientist at Occidental Petroleum, leading the research and deployment of large-scale computational models for subsurface applications. His research has been published in leading, high impact journals. He was awarded the

...